Title: Experimental investigation on the controls of clumped isotopologue and hydrogen isotope ratios in microbial methane

Authors and affiliations:
Danielle S. Gruen[1,2,*], David T. Wang[1,2,+], Martin Könneke[3], Begüm D. Topçuoğlu[4], Lucy C. Stewart[4,^], Tobias Goldhammer[3,5], James F. Holden[4], Kai-Uwe Hinrichs[3], and Shuhei Ono[1,*]

[1]Department of Earth, Atmospheric and Planetary Sciences, Massachusetts Institute of Technology, Cambridge, Massachusetts 02139, USA.
[2]Marine Chemistry and Geochemistry Department, Woods Hole Oceanographic Institution, Woods Hole, Massachusetts 02543, USA.
[3]MARUM Center for Marine Environmental Sciences and Department of Geosciences, University of Bremen, Bremen D-28359, Germany.
[4]Department of Microbiology, University of Massachusetts, Amherst, Massachusetts 01003, USA.
[5]Leibniz-Institute for Freshwater Ecology and Inland Fisheries, Department of Chemical Analytics and Biogeochemistry, Mueggelseedamm 301, 12587 Berlin, Germany
[+]Present address: ExxonMobil Upstream Research Company, Spring, TX 77389, USA.
[^]Present address: GNS Science, Lower Hutt 5010, New Zealand.

*To whom correspondence should be addressed:
Danielle Gruen (dgruen@mit.edu),
Shuhei Ono (sono@mit.edu)
Department of Earth, Atmospheric, and Planetary Sciences
Massachusetts Institute of Technology
77 Massachusetts Ave, Cambridge, MA 02139

Abstract

The abundance of methane isotopologues with two rare isotopes (e.g., $^{13}CH_3D$) has been proposed as a tool to estimate the temperature at which methane is formed or thermally equilibrated. It has been shown, however, that microbial methane from surface environments and from laboratory cultures is characterized by low $^{13}CH_3D$ abundance, corresponding to anomalously high apparent $^{13}CH_3D$ equilibrium temperatures. We carried out a series of batch culture experiments to investigate the origin of the non-equilibrium signals in microbial methane by exploring a range of metabolic pathways, growth temperatures, and hydrogen isotope compositions of the media. We found that thermophilic methanogens (*Methanocaldococcus jannaschii, Methanothermococcus thermolithotrophicus,* and *Methanocaldococcus bathoardescens*) grown on H_2+CO_2 at temperatures between 60 and 80°C produced methane with $\Delta^{13}CH_3D$ values (defined as the deviation from stochastic abundance) of 0.5 to 2.5‰, corresponding to apparent $^{13}CH_3D$ equilibrium temperatures of 200 to 600°C. Mesophilic methanogens (*Methanosarcina barkeri* and *Methanosarcina mazei*) grown on H_2+CO_2, acetate, or methanol produced methane with consistently low $\Delta^{13}CH_3D$ values, down to -5.2‰. Closed system effects can explain part of the non-equilibrium signals for methane from thermophilic methanogens. Experiments with *M. barkeri* using D-spiked water or D-labeled acetate (CD_3COO^-) indicate that 1.6 to 1.9 out of four H atoms in methane originate from water, but $\Delta^{13}CH_3D$ values of product methane only weakly correlate with the D/H ratio of medium water. Our experimental results demonstrate that low $\Delta^{13}CH_3D$ values are not specific to the metabolic pathways of methanogenesis, suggesting that they could be produced during enzymatic reactions common in the three methanogenic pathways, such as the reduction of methyl-coenzyme M. Nonetheless C-H bonds inherited from precursor methyl groups may also carry part of non-equilibrium signals.

1. Introduction

Methane is significant to the global carbon cycle (e.g., Alperin and Blair, 1992), a potent greenhouse gas (e.g., Wecht and Jacob, 2014), a source of energy (e.g., Whiticar, 1990), and a potential biosignature both for the deep biosphere (e.g., Inagaki et al., 2015) and planetary missions (e.g., Webster et al., 2014). The greatest natural source of methane to the atmosphere is produced by microbes in anoxic environments such as swamps, sediments, rice paddies, and ruminant tracts (Klapp et al., 2010). Microbial methanogenesis also contributes the majority of methane to oceanic gas hydrates, the largest reservoir of methane on Earth (Kvenvolden, 1993; Thauer et al., 2008).

Three major pathways are known for microbial methanogenesis (Thauer, 1998):

Hydrogenotrophic methanogenesis $CO_2 + 4H_2 \rightarrow CH_4 + 2H_2O$ (1)

Acetoclastic methanogenesis $CH_3COOH \rightarrow CH_4 + CO_2$ (2)

Methylotrophic methanogenesis $4CH_3OH \rightarrow 3CH_4 + CO_2 + H_2O$ (3)

Hydrogenotrophic methanogenesis (1) is the reduction of CO_2 with H_2 as an electron donor, which is employed by at least six of the seven known orders of methanogens (Bapteste et al., 2005). Although not as common, methanogens capable of hydrogenotrophic methanogenesis can use formate as both a source of carbon and as electron donor (Bapteste et al., 2005). Acetoclastic methanogenesis (2), the disproportionation of acetate to CH_4 and CO_2, is restricted to the genera *Methanosarcina* and *Methanosaeta* within the order Methanosarcinales. Hydrogenotrophic and acetoclastic methanogenesis are the two most common forms of microbial methanogenesis today (Conrad, 2005). Methylotrophic methanogenesis (3), used by Methanosarcinales and Methanomassiliicoccales, uses methyl compounds (e.g., methanol, methyl amines, dimethylsulfide, or methylthiols) as substrates (Bapteste et al., 2005; Penger et al., 2012). Nonetheless, all methanogenic archaea possess the enzyme methyl-coenzyme M reductase (MCR) which catalyzes the final step of methanogenesis (e.g., Ermler et al., 1997; Grabarse et al., 2000; Scheller et al., 2013; Wagner et al., 2016).

Carbon ($^{13}C/^{12}C$) and hydrogen (D/H) isotope ratios have been widely used to identify the origin of methane in the environment (Blair and Carter, 1992; Whiticar, 1999; Conrad et al., 2009; McCalley et al., 2014; Blaser and Conrad, 2016). However, it is often challenging to accurately determine the methane source since the isotopic composition of methane depends upon carbon and hydrogen sources as well as isotope fractionation during formation processes (Waldron et al., 1999; Valentine et al., 2004; Yoshioka et al., 2008; Kawagucci et al., 2014).

Previous culture experiments using D-labeled water (Daniels et al., 1980) or D-spiked water (Kawagucci et al., 2014) indicate that hydrogen in hydrogenotrophic methane is primarily derived from the hydrogen in water with only minor contribution from hydrogen in hydrogen gas (H_2). The contribution from H_2 can be explained by the production of metabolic water (Sugimoto and Wada

1995) since the production of one mole of methane yields two moles of water ($CO_2+4H_2 \rightarrow CH_4+2H_2O$), and the high specific rate of methanogenesis results in rapid turnover of intracellular water. The residence time of intracellular water is estimated to be as short as a few seconds (much lower than the doubling time of cells) during exponential growth (Kawagucci et al., 2014). The δD value of intracellular water can also be influenced by exchange between H_2 and H_3O^+, which can be catalyzed by hydrogenase enzymes (Burke, 1993; Valentine et al., 2011). Alternatively, the direct transfer of hydrogen in H_2 into CH_4 can be mediated by the enzyme methylenetetrahydromethanopterin dehydrogenase (Schworer et al., 1993; Schleucher et al., 1994; Klein et al., 1995a,b; Hartmann et al., 1996). In contrast, experiments with acetoclastic methanogens indicate that up to three out of four hydrogen atoms in methane are derived from the methyl group of acetate, as implied in the stoichiometry of Reaction (2) (Pine and Barker, 1956).

In addition to the ratios of $^{13}C/^{12}C$ and D/H of methane, measurements of the doubly isotope substituted isotopologue, $^{13}CH_3D$ and/or $^{12}CH_2D_2$, have recently been applied as tools to constrain the source of methane in a variety of environments (Stolper et al., 2013; Stolper et al., 2014; Wang et al., 2015; Douglas et al., 2016; Wang et al., 2016; Young et al., 2016; Douglas et al., 2017; Whitehill et al., 2017; Young et al., 2017). The following reaction shows the equilibrium among four methane isotopologues, including $^{13}CH_3D$:

$$^{13}CH_4 + {}^{12}CH_3D \leftrightarrow {}^{13}CH_3D + {}^{12}CH_4. \qquad (4)$$

Here, its equilibrium constant (K_T) can be written as:

$$K_T = \frac{[^{13}CH_3D][^{12}CH_4]}{[^{12}CH_3D][^{13}CH_4]}. \qquad (5)$$

The value of K_T primarily depends on temperature, and it approaches unity at high temperatures (1.0002 at 1,000°C), but is about 1.0057 at 25°C as estimated by molecular simulations (Ma et al., 2008; Stolper et al., 2015; Wang et al., 2015; Liu and Liu, 2016). Thus, the precise measurements of four isotopologues' abundance ($^{12}CH_4$, $^{13}CH_4$, $^{12}CH_3D$, and $^{13}CH_3D$) were thought to provide an estimate of the temperature at which the methane gas was formed or thermally equilibrated. Initial studies using high-resolution mass-spectrometry demonstrated that this new isotopologue thermometer provides a range of temperatures that are consistent with formation temperatures for methane samples from geologic environments, such as natural gas reservoirs (Stolper et al., 2014). Later studies, however, showed that methane sampled from surface environments (e.g., ruminants, lakes, and swamps) is characterized by clear non-equilibrium signals that yield apparent clumped isotopologue temperatures higher than environmental methane generation temperatures (Stolper et al., 2015; Wang et al., 2015; Douglas et al, 2016; Young et al., 2017).

These studies also showed that the degree of methane isotopologue disequilibrium is correlated with D/H-isotope disequilibrium between H_2O and CH_4 (i.e., $CH_3D + H_2O \leftrightarrow CH_4 + HDO$). To explain this observed relationship, Wang et al. (2015), and Stolper et al. (2015) both presented a mathematical model that considered metabolic reversibility, which is defined as the ratio of backward to forward fluxes through an enzymatically-mediated reaction sequence. These models were based on earlier models for sulfur isotope effects of sulfate reducers (Rees, 1973; Farquhar et al., 2007; Sim et al., 2011). By choosing the appropriate fractionation factors, these models can describe isotopologue compositions of microbial methane between kinetic and equilibrium end-members, corresponding to unidirectional and reversible reactions, respectively. Accordingly, both studies attributed the origin of kinetic clumped isotope signals intrinsic to one or more enzymatic reactions in the methanogenic pathways. The application of transition state theory (Bigeleisen, 1949) can explain $^{13}CH_3D$ abundance between equilibrium and stochastic ($\Delta^{13}CH_3D$ >0‰), but anti-clumped $^{13}CH_3D$ abundance ($\Delta^{13}CH_3D$ <0‰) requires the mixing of methane reservoirs with an often unreasonably large range of bulk δD and $\delta^{13}C$ values or a physical mechanism, including quantum mechanical tunneling (Wang et al., 2015; Whitehill et al., 2017; Young et al., 2017) ($\Delta^{13}CH_3D$ is a measure of excess $^{13}CH_3D$ as defined later in equation (8)). For the doubly deuterated isotopologue CH_2D_2, purely statistical combinational-effects can also produce large apparent depletions in CH_2D_2 (Yeung et al., 2016, Young et al., 2017).

Recent work cultivating methanogens produced isotopologue compositions consistently out of isotopic equilibrium (Douglas et al., 2016; Young et. al., 2017). These results were in agreement with previous culture studies (Stolper et al., 2015; Wang et al., 2015), but highlighted the need for further assessment of the mechanisms that control microbial $^{13}CH_3D$ compositions. In particular, the source of H in CH_4 for acetoclastic and methylotrophic methanogenesis remained uncertain (Douglas et al., 2016, 2017). The goal of this work is to better characterize the kinetic $^{13}CH_3D$ effects that lead to these generally low $\Delta^{13}CH_3D$ values, specifically during microbial methanogenesis, using a comprehensive set of metabolic pathways and temperatures. We investigated this with a series of batch culture experiments to test the effect of 1) species (*Methanothermococcus thermolithotrophicus*, *Methanocaldococcus jannaschii*, *Methanocaldococcus bathoardescens, Methanosarcina barkeri*, and *Methanosarcina mazei*), 2) temperature (from 30 to 85°C), and 3) substrate (H_2+CO_2, acetate, and methanol). We also investigated the effect of closed-system processes as well as D/H ratios of medium water to test if apparent high-temperature signals are produced by mixing of two or more pools of methane (or its precursors), as mixing has been shown to produce a bias in the clumped isotopologue temperature estimate (Stolper et al., 2015; Wang et al., 2015; Douglas et al., 2016).

2. Methods

2.1 Laboratory Culture Experiments

Table 1 summarizes all culture experiments conducted in this study as well as results from our earlier experiments presented in Wang et al., (2015). Descriptions of specific experimental conditions are provided below.

2.1.1 Temperature Series Experiments

Pure cultures of methanogens were grown in duplicate in batch cultures at a range of temperatures (30 to 85°C). Three different hydrogenotrophic methanogens were selected based on their growth kinetics and optimum growth temperatures: *Methanothermococcus thermolithotrophicus*, *Methanocaldococcus jannaschii*, and *Methanocaldococcus bathoardescens.* Cultures of *M. thermolithotrophicus* and *M. jannaschii* were purchased from the German Collection of Microorganisms and Cell Cultures (DSMZ, Braunschweig, Germany). *M. bathoardescens* was originally isolated from vent fluid at Axial Volcano, Juan de Fuca Ridge, and maintained in culture at the University of Massachusetts, Amherst (Stewart et al., 2015).

Culture medium was prepared following the recipe for DSMZ medium 282 according to Stewart et al. (2015). The headspace was filled with H_2:CO_2 (in a ratio of 80:20 by volume) at 2 bar absolute pressure. For each experiment, 5 mL of inoculum from a culture in the exponential growth phase was added to a sample vial containing 50 mL media. *M. thermolithotrophicus* was grown at 30, 40, 50, and 60°C, *M. jannaschii* was grown at 70 and 80°C, and *M. bathoardescens* was grown at 85°C. All cultures were incubated in 140 mL rubber-stoppered glass serum vials in forced-air convection ovens. Cell concentrations were monitored by cell counts with a Petroff-Hauser counting chamber and phase-contrast light microscope to determine the growth kinetics as a function of temperature (Stewart et al., 2016). Experiments for isotope measurement were stopped at a time when stationary phase was reached (5 to 64 hours, as measured in prior studies and replicated in our laboratory (Huber et al., 1982, Jones et al., 1983, Ver Eecke et al., 2013); Table 2). Most CO_2 (>95%) was converted to CH_4 as indicated by gas chromatography (GC) measurements of carbon dioxide and methane in the headspace gas.

2.1.2 Time Series Experiments

M. bathoardescens was grown under an H_2:CO_2 (80:20) atmosphere in replicate batch cultures at 80°C to study the effects of growth phase and closed system on $^{13}CH_3D$ and to estimate instantaneous clumped isotopologue fractionation factors. Culture medium was prepared as above (Sec. 2.1.1). Methane was sampled and analyzed by GC from batch cultures at time points

corresponding to fractional conversion of 6, 10, 68, and 77% of the initial carbon dioxide to methane (Table 1). The fractional conversion was calculated by dividing the volume of methane produced at the conclusion of the experiment by the volume of methane expected.

2.1.3 Substrate Series Experiments

To determine the effect of different metabolic pathways, established batch culture incubations of *Methanosarcina barkeri* were grown on three different substrates: H_2+CO_2, (referred to as hydrogenotrophic cultures hereafter), methanol (methylotrophic cultures), and acetate (acetoclastic cultures). Cultures of *M. barkeri* (strain DSM-800) were purchased from the DSMZ (Braunschweig, Germany). The growth medium was prepared according to the recipe for DSMZ medium 120 (Balch et al., 1979). For hydrogenotrophic cultures, the headspace was filled with 1.5 absolute bar of H_2:CO_2 (80:20) gas mix. For acetoclastic and methylotrophic cultures, the headspace was filled with 1.5 absolute bar of N_2:CO_2 (70:30) gas mix and the medium was amended with 30 mM of Na-acetate or 250 mM of methanol, respectively. Cultures were incubated in duplicate near room temperature. Two sets of experiments were carried out. The first set of experiments (Set 1) was intended to provide preliminary data, and thus temperature was not strictly controlled over the course of the experiment (cultures exposed to ambient temperatures between 21 and 38°C), and the medium contained yeast extract. Nonetheless, all bottles in this series were subjected to identical environmental conditions. A second set of cultures (Set 2) was prepared and incubated under close monitoring at constant temperature (38°C). Yeast extract (YE) and casitone were omitted from medium unless otherwise noted. At the end of the experiment, cultures were killed with 1M NaOH to prevent any additional methanogen activity as described in Methods Section 2.2.

2.1.4. D-label and d-spike Experiments

To constrain the source of hydrogen in the hydrogenotrophic, methylotrophic, and acetoclastic pathways, a subset of *M. barkeri* cultures was also spiked with either 15 or 30 µL of D_2O per one liter of media. Additionally, acetoclastic cultures were prepared containing 10, 50, or 100% (molar fraction) deuterated acetic acid (CD_3COOD, 99% purity, Sigma-Aldrich, St. Louis, MO).

2.2 Sample Preparation and Isotopologue measurements

At the completion of an experiment, 1 M NaOH was injected in each culture bottle (at a ratio of 1 mL per 10 mL of medium) to sacrifice the culture and to draw down CO_2 pressures in the headspace. Methane samples from culture experiments were measured within one year of the completion of culture experiments. Repeated measurements of NaOH-treated samples did not

show measureable changes in isotope or isotopologue ratios during storage. The headspace was sampled by flushing with helium via two needles. Methane gas was purified from culture gas mixtures (mostly methane, hydrogen, and nitrogen) using an automated preparative gas chromatography system as previously described (Wang et al., 2015). For most analyses, approximately 10 mL STP of methane was used.

The abundance of isotopologues in methane samples was measured by a tunable infrared laser direct absorption spectrometer (TILDAS) that measures absorption in the infrared region of the electromagnetic spectrum corresponding to bending vibrations of C–H and C–D bonds (Ono et al., 2014; Wang et al., 2015). A typical measurement consists of eight to ten cycles of alternating measurements of reference and sample methane. Measured isotopologue ratios were averaged and 95% confidence intervals were calculated according to Student's *t*-distribution as previously described (Wang et al., 2015).

The hydrogen isotope composition of culture medium water (δD_{H2O}), except for that of *Methanosarcina* Set 2 experiments, was measured using a cavity ring-down spectrometer (CRDS, Picarro Inc., Santa Clara, California, USA) at the University of Massachusetts, Amherst. The δD_{H2O} values of the *Methanosarcina* Set 2 cultures were measured at the University of Bremen also by CRDS (Picarro L2130-*i* Analyzer (Picarro Inc., Santa Clara, CA, USA). The hydrogen isotope composition of H_2 was not measured. Bulk $\delta^{13}C$ of methanol and acetate were measured via LC-IRMS at the University of Bremen (Heuer et al., 2006). CO_2 in the N_2:CO_2 and H_2:CO_2 gas mixes, bicarbonate solution, and culture media were measured via isotope ratio infrared spectrometry (IRIS) at the University of Bremen. The D/H ratio of sodium acetate (CH_3COONa) was measured by high temperature conversion elemental analyzer interfaced with isotope ratio mass-spectrometer (IRMS) at University of Chicago. Typical uncertainties were 0.2 to 0.4‰ and 2 to 5‰ for $\delta^{13}C$ and δD, respectively.

2.3. Isotope Notation and Calibration

In this work, stable isotopic ratios of carbon and hydrogen are reported in conventional δ notation, defined as:

$$\delta^{13}C = \frac{(^{13}C/^{12}C)_{sample}}{(^{13}C/^{12}C)_{PDB}} - 1 \qquad (6)$$

$$\delta D = \frac{(D/H)_{sample}}{(D/H)_{SMOW}} - 1 \qquad (7)$$

where, PDB and SMOW are Pee Dee Belemnite and Standard Mean Ocean Water, respectively. The factor of 1000, which commonly appears in definitions of δ values in the geochemical literature, has been omitted from Equations (6) and (7), as it is implied by the permil (‰) symbol, in accordance with IUPAC recommendations (Coplen, 2011). Values for $\delta^{13}C$ and δD of methane

analyzed via TILDAS at MIT have been calibrated against PDB and SMOW via measurements of natural gas standards NGS-1 and NGS-3 (Wang et al., 2015). Reference values for $\delta^{13}C$ and δD were taken to be −29.0‰ and −138‰ for NGS-1, and −72.8‰ and −176‰ for NGS-3, respectively (Hut, 1987).

Because the TILDAS measures ratios of methane isotopologues, bulk $\delta^{13}C$ and δD values reported in this paper are necessarily derived quantities. For samples of methane containing a mix of isotopologues at or sufficiently close to their naturally-occurring abundances, including all samples analyzed via TILDAS in this study, ratios of isotopologues are interchangeable with ratios of isotopes (i.e., $^{13}C/^{12}C$ and D/H) when calculating δ values, with no difference within achievable uncertainties of isotope ratio measurements: $^{13}C/^{12}C \approx [^{13}CH_4]/[^{12}CH_4]$ and $D/H \approx ¼ [^{12}CH_3D]/[^{12}CH_4]$. Note that the symmetry factor of ¼ cancels out when δD values are calculated via equation (7).

The abundance of the clumped isotopologue $^{13}CH_3D$ is reported as $\Delta^{13}CH_3D$, which represents the deviation (excess) of the abundance of $^{13}CH_3D$ from a stochastic distribution (i.e., one in which all carbon and hydrogen isotopes are randomly distributed amongst the isotopologues $^{12}CH_4$, $^{13}CH_4$, $^{12}CH_3D$, and $^{13}CH_3D$) (Ono et al., 2014):

$$\Delta^{13}CH_3D = \frac{[^{13}CH_3D][^{12}CH_4]}{[^{13}CH_4][^{12}CH_3D]} - 1$$

$$\cong \ln\frac{^{13}CH_3D}{^{12}CH_4} - \ln\frac{^{13}CH_4}{^{12}CH_4} - \ln\frac{^{12}CH_3D}{^{12}CH_4}. \quad (8)$$

We used the following equation to derive apparent $\Delta^{13}CH_3D$ temperatures:

$$\Delta^{13}CH_3D(T) = -0.1101\left(\frac{1000}{T}\right)^3 + 1.0415\left(\frac{1000}{T}\right)^2 - 0.5223\left(\frac{1000}{T}\right) \quad (9)$$

where T is in Kelvin. Density function theory (B3LYP) with 6-31G(d) basis set was used to estimate harmonic vibrational frequencies, and isotope fractionation factors were calculated following conventional theory by Urey (1947). A sample of methane with stochastically-distributed abundances of isotopologues has a $\Delta^{13}CH_3D$ value of zero, corresponding to an apparent equilibrium temperature of infinity for Reaction (4). Negative $\Delta^{13}CH_3D$ values represent "anti-clumped" signals, where the abundance of $^{13}CH_3D$ is more depleted than that expected for stochastic isotopologue distribution.

Measurements made via TILDAS give the abundances of methane isotopologues relative to a reference gas against which the samples are measured (here, a commercially-sourced cylinder of methane termed "AL1" was used as the reference gas). To express $\Delta^{13}CH_3D$ values of samples relative to the stochastic distribution requires determination of the $\Delta^{13}CH_3D$ value of the reference gas AL1. This was determined by heating AL1 in a flame-sealed glass tube in the presence of a

platinum catalyst between 150 and 400°C for several days to months (Ono et al., 2014; Wang et al., 2015).

The fractionation factor (α) quantifies the difference in the relative abundance of isotopes between the substrate and the instantaneous product of a reaction. For the reduction of carbon dioxide to methane, the fractionation factor is defined as:

$$^{13}\alpha_{CH4/CO2} = \frac{\delta^{13}C_{CH4} + 1}{\delta\ ^{13}C_{CO2} + 1}. \qquad (10)$$

Two modes of D/H fractionation characterize each hydrogen addition step during the biosynthesis of methane. For example, for addition of H (or D) onto a methyl group:

$$CH_3\text{-}R_1 + D\text{-}R_2 \rightarrow CH_3D + R_1\text{-}R_2 \qquad ^2\alpha_p \qquad (11)$$

$$CH_2D\text{-}R_1 + H\text{-}R_2 \rightarrow CH_3D + R_1\text{-}R_2 \qquad ^2\alpha_s \qquad (12)$$

Reaction (11) is accompanied by a *primary* D/H isotope effect (characterized by the fractionation factor $^2\alpha_p$), where a D is substituted for H in the bond formed (or broken). Reaction (12) is accompanied by a *secondary* D/H isotope effect (with fractionation factor $^2\alpha_S$), where the substitution of D for H occurs on the site *adjacent* to the C–H bond being formed (or broken) and the C–D bond are carried from reactant to product. Primary D/H isotope effects are typically much larger compared to secondary isotope effects. For the reduction of methyl-coenzyme M to methane above, the secondary isotope effect is 0.84 and the primary isotope effect of the backward reaction is 0.41 (Scheller et al., 2013).

According to the rule of geometric mean (Bigeleisen, 1955), the fractionation factor for the clumped isotopologue $^{13}CH_3D$ is usually close, but not necessarily equal, to the product of carbon and hydrogen fractionation factors ($^{13\text{-}2}\alpha \simeq {}^{13}\alpha^2\alpha$). A significant departure from this rule has been observed for some *in vitro* enzyme assay experiments for doubly deuterated substrates, and attributed to quantum mechanical tunneling (e.g., Srinvasan et al., 1985; Amin et al., 1988; Huskey et al., 2007). We represent the departure from this relationship by the γ factor, which is a metric of the kinetic clumped isotope effect (Wang et al., 2015). There are two ways by which a ^{13}C-containing methyl group can acquire an H (or D) to form $^{13}CH_3D$ (analogous to Reactions 5 and 6). Thus, there are two γ factors corresponding to primary (γ_P) and secondary D/H isotope effects (γ_S):

$$^{13\text{-}2}\alpha_P = \gamma_P\ {}^{13}\alpha^2\alpha_P \text{ and} \qquad (13)$$

$$^{13\text{-}2}\alpha_S = \gamma_S\ {}^{13}\alpha^2\alpha_S. \qquad (14)$$

For bond forming reactions, product methane could become anti-clumped ($\Delta^{13}CH_3D<0$) when the value of γ is less than unity.

2.4 FTIR Analysis of Methane Isotopologues

A Fourier transform infrared (FTIR) spectrometer (iS5, Thermo Scientific, Waltham, Massachusetts, USA) was used to quantify the mixing ratios of deuterated isotopologues of

methane (CHD_3, CH_2D_2 and CH_3D) and non-deuterated methane (CH_4), produced in acetoclastic cultures spiked with CD_3COOD. The FTIR spectrometer has a 0.8 cm^{-1} spectral resolution, and is equipped with a gas cell that has a path length of 10 cm, volume of 70 mL, and windows of KBr. The cell was evacuated and filled with argon three times prior to injection of the sample or standard. For each measurement, 100 µL to 1 mL standard temperature and pressure (STP) of the standard or sample (culture headspace, subsampled with a gas-tight syringe, Vici Valco, Houston, Texas, USA) was injected into the cell through a small inlet valve. Reference spectra were taken on samples of ordinary CH_4 (containing D at natural abundance) and on pure (>98% purity) deuterated isotopologues (CH_3D, CH_2D_2, and CD_3H) purchased from Cambridge Isotope Laboratories (Cambridge, MA). The mixing ratio of methane isotopologues was determined by a least squares fit in the region of the absorption spectrum between 3200 and 2800 cm^{-1}.

3. Results

Table 1 (Section 2) summarizes the tables and figures in which results for each set of methanogen culture experiments are displayed, Table 2 summarizes all data used in the figures that follow, and Table 3 summarizes the isotope composition of substrates and medium water.

3.1 Non-equilibrium $\Delta^{13}CH_3D$ signals of methane from microbial cultures

Microbial methane produced from pure culture experiments yielded non-equilibrium signals with corresponding apparent clumped isotope temperatures much higher than the temperatures at which the cultures were incubated (Figure 1). Overall, thermophilic methanogens (grown at >40°C) produced $\Delta^{13}CH_3D$ values that are lower than those expected for equilibrium distribution (0.5 to 2.5‰), whereas mesophilic methanogens produced lower (mostly anti-clumped) signals (-5.2 to 1.6‰), consistent with limited measurements reported in Douglas et al., (2016) and Young et al., (2017).

Thermophilic methanogens (*M. jannaschii, M. bathoardescens,* and *M. thermolithotrophicus*) grown on H_2+CO_2 between 30 and 80°C produced methane with $\Delta^{13}CH_3D$ values ranging from 2.5 to 0.5‰, corresponding to apparent clumped isotopologue temperatures of 195 to 603°C, respectively. Methane produced by *Methanosarcina* (*M. barkeri* and *M. mazei*) grown on H_2+CO_2, acetate, and methanol was characterized by $\Delta^{13}CH_3D$ values ranging from -5.2 to -1.1‰, which are lower than those of methane produced by thermophilic methanogens (Figure 1).

As described in the methods (Section 2.1.3), Set 1 cultures were exposed to ambient temperatures between 21 and 38°C and the media contained yeast extract. Set 2 cultures were prepared and incubated under close monitoring at constant temperature (38°C). Yeast extract (YE) and casitone were omitted from media unless otherwise noted (Table 2), and at the end of the experiment, cultures were killed with 1M NaOH. There are some notable differences in the $\Delta^{13}CH_3D$ values between Set 1 and Set 2 experiments for cultures with *M. barkeri* and *M. mazei*. Table 2 shows that Set 1 exhibits slightly higher $\Delta^{13}CH_3D$ values for each substrate, most extreme for cultures grown on H_2+CO_2 (as much as a 3‰ difference). *M. barkeri* cultures in Set 2 grown on H_2+CO_2 at lower temperatures (21 vs. 38°C) but in the same conditions without any isotope spike exhibit higher $\Delta^{13}CH_3D$ values (by 2.0‰).

Because methanogens grown on different substrates and at different temperatures exhibit different growth rates, methane was generated more quickly or slowly for some bottles. For the Time Series experiments (TS), the culture headspace reached <1% CO_2 in as little as 5 hours for 80°C cultures and as long as 3 days for 30°C cultures. Cultures in the Time Series experiments (CS) were stopped intervals between 2.75 and 4 hours, spanning 6-77% reaction completion (Table 2). Methanogens from the Substrate, Spike, and Temperature experiments (1&2) took much longer to generate methane. Set 2 cultures required long as two months of incubation in order to produce enough methane to be sampled and analyzed.

3.2 Effect of a closed system on $\delta^{13}C$, δD_{CH4}, and $\Delta^{13}CH_3D$ systematics

In order to test the potential bias in $\Delta^{13}CH_3D$ values due to closed system isotope effects, methane was sampled from batch cultures in time series experiments (Table 2; Figure 2). The $\delta^{13}C$ value of methane increased from -18.0 to -3.8‰ over the course of experiments (Figure 2A). This increase is consistent with closed system isotope effects. In contrast, δD values of methane decreased (-350.3 to -402.3‰) over the course of the experiment (Figure 2B). Our results show $\Delta^{13}CH_3D$ values remain relatively constant over the course of the experiment between 2.1 and 2.5‰ (Figure 2C).

3.3 D-spiked H_2O experiments

As the δD of water is increased by spiking the media water, the δD of product methane also increased (Figure 3). This illustrates the uptake of hydrogen from water to form methane, consistent with previous pure culture (Yoshioka et al., 2008; Kawagucci et al., 2014; Okumura et al., 2016) and incubation experiments (Schoell, 1980; Sugimoto and Wada, 1995). Linear

regression of the data for hydrogenotrophic, acetoclastic, and methylotrophic cultures yielded the following relationships, respectively:

$$\delta D_{CH4} = (0.571\pm0.011)\ \delta D_{H2O} - (423.0\pm2.1), \quad (15)$$

$$\delta D_{CH4} = (0.212\pm0.004)\ \delta D_{H2O} - (331.5\pm0.8), \text{ and} \quad (16)$$

$$\delta D_{CH4} = (0.269\pm0.005)\ \delta D_{H2O} - (369.7\pm1.2). \quad (17)$$

where intercepts are in ‰. The linear fit and standard error for the slope and intercept was calculated following (York et al., 2004) by taking into account standard errors of 0.2‰ and 5‰ for δD_{CH4} and δD_{H2O} (assuming errors are not correlated). Hydrogenotrophic cultures yielded a higher slope (0.571) compared to methylotrophic (0.269) and acetoclastic (0.211) cultures.

The values of $\Delta^{13}CH_3D$ are weakly dependent on pathways: -2.9 to -3.8‰, -4.2 to -4.9‰, and -2.4 to -3.1‰ for hydrogenotrophic, methylotrophic, and acetoclastic cultures, respectively. For each pathway, lower $\Delta^{13}CH_3D$ values tend to be associated with lower δD_{H2O} values (Figures 3 and 4). The linear fit and standard error for the slope and intercept was calculated as described above. Hydrogenotrophic cultures yielded a higher slope (0.0020±0.0010) compared to methylotrophic (0.0019±0.0014) and acetoclastic (0.0016±0.0012) cultures.

3.4 D-labeled acetate experiment

In order to track the transfer of D (or H) from the methyl group of acetate to methane, *M. barkeri* was cultured with medium spiked with CD_3COO^-. As the amount of CD_3COO^- in an acetoclastic methanogen culture increased, not only the relative abundance of CHD_3 but also that of CH_2D_2 and CH_3D increased at the expense of CH_4 (Figure 4). Cultures incubated with 100% CD_3COO^- produced methane comprised of a majority of triply deuterated isotopologues (68% CHD_3) but also contained CH_2D_2, (13%) and CH_3D (5%).

4. Discussion

4.1 Closed system isotope effect does not explain non-equilibrium $\Delta^{13}CH_3D$

Methanogens in the temperature series experiment (Method 2.1) were incubated until nearly all the substrate (CO_2) had been converted to product (CH_4). As a result, the $\delta^{13}C$ value of the product methane would have increased with reaction progress, eventually reaching the $\delta^{13}C$ value of the starting CO_2. In addition to changes in δ values due to closed system effects, it has been shown that the apparent D/H fractionation factor between methane and water changes with

growth phase (Valentine et al., 2004; Kawagucci et al., 2014). This could be due to changes in the δD value of intracellular water via D/H exchange with H_2 (Burke, 1996) or the contribution from metabolic water (Kawagucci et al., 2014). Values of $\Delta^{13}CH_3D$ do track non-linearly with $\delta^{13}C$ and δD upon the mixing of two or more pools of methane (Stolper et al., 2015; Wang et al., 2015; Douglas et al., 2016), such that mixing of two methane reservoirs would result in non-equilibrium $\Delta^{13}CH_3D$ values even when $\Delta^{13}CH_3D$ values of the source reservoirs carry equilibrium signals. We sought to isolate any experimental effects introduced in the closed system and therefore tested if changing the $^{13}C/^{12}C$ and/or D/H ratios of bulk methane over the course of the reaction may also affect the $\Delta^{13}CH_3D$ value of the end product.

The production of four methane isotopologues from two isotopologues of CO_2 can be written as:

$$^{12}CO_2 \rightarrow {}^{12}CH_4, \qquad k \qquad (18)$$

$$^{13}CO_2 \rightarrow {}^{13}CH_4, \qquad {}^{13}\alpha\, k \qquad (19)$$

$$^{12}CO_2 \rightarrow {}^{12}CH_3D, \qquad {}^{2}\alpha\, R_H\, k \qquad (20)$$

$$^{13}CO_2 \rightarrow {}^{13}CH_3D, \qquad \gamma\, {}^{13}\alpha {}^{2}\alpha R_H\, k \qquad (21)$$

where, k is the pseudo-first order rate constant for $^{12}CO_2$ to $^{12}CH_4$, $^{13}\alpha$ and $^{2}\alpha$ are the carbon and hydrogen isotope fractionation factors, respectively, and R_H is the D/H ratio of source hydrogen (intracellular water, $R_H = R_{SMOW}(\delta D_{H2O}+1)$). For the application of equation (20) and (21), we assume that the source for H of CH_4 is intracellular water. The value of δD of intercellular water can be different from that of media due to exchange with H_2 or production of metabolic water inside the cytoplasm (Burke, 1993; Kawagucci et al., 2014). In addition, the direct transfer of H in H_2 to CH_4 was suggested (Kawagucci et al., 2014). Since the detailed mechanism of the effect of δ D-H_2 is beyond the scope of this study, the above model includes the effect as the change of the $^{2}\alpha$ value during the course of the culture. Changing R_H would produce results identical to changing $^{2}\alpha$. Equations (18) to (21) were integrated numerically with three fitting parameters ($^{13}\alpha$, $^{2}\alpha$, and γ), and the results are shown in Figure 2. We used $\delta^{13}C$ and δD data to fit $^{13}\alpha$ and $^{2}\alpha$, and the $\Delta^{13}CH_3D$ data was used to fit γ value for the derived $^{13}\alpha$ and $^{2}\alpha$ values.

The best fit to the experimental data was obtained when $^{13}\alpha$ was 0.97 and $^{2}\alpha$ changed linearly from 0.69 to 0.57 from 0 to 25% reaction and remained a constant value of 0.57 afterwards (Figure 2 A and B) (δD_{H2O} of -49.6‰ SMOW, and $\delta^{13}C_{CO2}$ of 10.9‰). As δD_{H2O} does not change significantly during the course of the experiment, the change in δD_{CH4} cannot be explained by the closed system effect. The increasing fractionation factor at a later stage indicates δD_{CH4} is moving away from the value expected for equilibrium with water. Previous studies also observed similar changes in apparent D/H fractionation factors during early exponential growth phases (Valentine et al., 2004; Kawagucci et al., 2014; Okumura et al., 2016). Values of δD of methane produced during the early growth phase can be a function of δD_{H2} as well as δD_{H2O} (Kawagucci et al., 2014).

For those $^{13}\alpha$ and $^{2}\alpha$ values, the best fit for γ was 1.0020 and 1.0032 for the early and late growth phases, respectively (Figure 2). The value of γ of higher than unity indicates that the rate of $^{13}CH_3D$ production is faster than the rate expected from the product of the two fractionation factors ($^{13}\alpha$ $^{2}\alpha$).

These derived γ values of 1.0020 and 1.0032 translate to closed-system corrected $\Delta^{13}CH_3D$ values of 2.0 and 3.2‰ respectively (corresponding to 243 and 135°C, for apparent equilibrium temperatures). These values are similar to the uncorrected values of 2.1 to 2.5‰, demonstrating that the effect of a closed system can only partially explain the non-equilibrium $\Delta^{13}CH_3D$ signals of microbial methane. The numerical model above shows that the $\Delta^{13}CH_3D$ value of accumulated methane decreases by up to 1.2‰ over the course of reaction given constant γ values, due to the effect of mixing of methane formed during early and late exponential growth phases (Figure 2C).

4.2 Origin of H in methane from three methanogenesis pathways

The results of the D-spiked series experiments can be used to estimate the origin of C-H bonds in methane during three pathways of methanogenesis and associated deuterium isotope effects ($^{2}\alpha_p$ and $^{2}\alpha_s$). Assuming methane is formed via mixing of hydrogen atoms both from H_2O and the methyl group of acetate or methanol, the δD value of product methane can be written as:

$$\delta D_{CH4} + 1 = {}^{2}\alpha_p f (\delta D_{H2O} + 1) + {}^{2}\alpha_s (1-f) (\delta D_{CH3} + 1) \quad (22)$$

where, $^{2}\alpha_p$ is the kinetic fractionation factor from H_2O to CH_4 (primary D-isotope effect), and $^{2}\alpha_s$ is the kinetic isotope fractionation factor from CH_3 (methyl-H) to CH_4 (secondary D-isotope effect) (Sessions and Hayes, 2005). The value of f is the fraction of H from H_2O. The canonical value of f is 0.25, but this can be higher when scrambling of C-H bonds occurs between C-H and intercellular H_2O.

Our experimental results yield the following relationships for CO_2 + H_2, acetate and methanol cultures, respectively (Figure 5):

$$\delta D_{CH4} + 1 = (0.571 \pm 0.011) (\delta D_{H2O} + 1) + (0.006 \pm 0.012), \quad (23)$$

$$\delta D_{CH4} + 1 = (0.212 \pm 0.004) (\delta D_{H2O} + 1) + (0.457 \pm 0.005), \text{ and} \quad (24)$$

$$\delta D_{CH4} + 1 = (0.269 \pm 0.005) (\delta D_{H2O} + 1) + (0.361 \pm 0.006). \quad (25)$$

For hydrogenotrophic methanogenesis, a small (can be zero within standard error) intercept suggests all four hydrogen atoms are derived from water (i.e., f=1), and an α_p value of 0.571 is obtained, which is within the range of previous experiments 0.55 and 0.86 (Valentine et al., 2004; Yoshioka et al., 2008; Kawagucci et al., 2014; Okumura et al., 2016).

The acetate culture (equation 24) yields:

$$^{2}\alpha_p f = 0.211, \text{ and} \quad (26)$$

$$^{2}\alpha_s (1-f)(\delta D_{CH3} +1) = 0.457. \quad (27)$$

The methyl-H of acetate is measured as -123‰ (i.e., $\delta D_{CH3}+1 = 0.877$, Table 3). The two fractionation factors, α_p and α_s, are calculated for a given value of *f* in Figure 6. The equations (26 and 27) cannot provide a unique answer, as there are two equations with three unknowns (α_p, α_s and *f*). The likely range of values can be constrained, however, because isotope fractionation factors are expected to be normal (i.e., $\alpha_p <1$ and $\alpha_s <1$), and the value of *f* is between ¼ and 1. This yields a range of possible values: $0.449< {}^{2}\alpha_p <0.844$ and $0.695< {}^{2}\alpha_s <1.0$, and $0.25< f < 0.48$ (Figure 6). The secondary isotope effect for the formation of methane from methyl-coenzyme M (the last step of methanogenesis, utilized by all known methanogens Figure 7) is reported to be 0.84 (Scheller et al., 2013). For example, this value for $^{2}\alpha_s$, would yield f=0.39 and $^{2}\alpha_p$= 0.545. The analysis indicates that the value of *f* significantly deviates from the canonical value of 0.25, which is expected from the reaction stoichiometry. Therefore, this analysis suggests that among the four hydrogen atoms in methane, up to 1.9 hydrogen atoms (=0.48×4) are derived from water, whereas only one is required from reaction stoichiometry. Since δD_{CH3} of methanol was not measured, we cannot carry out the same analysis for methanol experiments. The slightly higher slope for methanol cultures (0.269) compared to acetate cultures (0.212), however, suggests a similar or greater contribution of hydrogen atoms from water if we assume the same $^{2}\alpha_p$ value for the acetate culture.

Previous incubation studies with D-spiked water showed slopes between δD_{CH4} and δD_{H2O} of 0.4 for sewage sludge (Schoell, 1980) and 0.48 to 0.61 for paddy soil (Sugimoto and Wada, 1995). These are higher than the value obtained by our experiments, indicating a higher contribution of water-H to methane in these incubation studies. Since previous experiments were enriched cultures (not pure cultures), results from previous experiments reflect a mixed contribution from hydrogenotrophic and acetoclastic methanogenesis. A previous incubation study of lake and estuary sediments using triply deuterated acetate (CD_3COO^-) showed rapid exchange of the methyl-H of acetate by methanogenic acetate metabolism (de Graaf et al., 1996). Such an exchange would contribute to the greater slope for the incubation study using natural populations, compared to pure culture experiments for this study.

4.3 Pathway of D-isotope exchange during acetoclastic methanogenesis

Figure 7 illustrates the three pathways of methanogenesis examined in this study. The solid arrows represent the predominant direction of reaction, and dashed arrows represent the backward reaction, which is thought to be minor. The two solid arrows are used where the reactions are

thought to be reversible. This reversibility was inferred from our results as well as based on previous studies (e.g., Thauer et al.,1998; Ferry 2010). Hydrogenotrophic methanogenesis proceeds with a series of two electron reactions, which each adding one H, while the C_1 group is carried by cofactors: methanofuran (MF), tetrahydrosarcinapterin (H_4SPT), and coenzyme M (CoM). Acetoclastic methanogenesis is a disproportionation reaction where acetate is activated to acetyl-coA (via acetyl phosphate) and split between a methyl and a carbonyl (CO) moiety, where the latter is oxidized to CO_2. The methyl group is transferred to CH_3-H_4SPT (methyl-tetrahydrosarcinaopterin), and then to CH_3-CoM (methyl-coenzyme M), and finally reduced to methane. Methylotrophic methanogenesis is also a disproportionation reaction where the oxidation of one methyl group is coupled with the reduction of three methyl groups. The last step (the reduction of methyl-CoM) is common to all three pathways, and most (if not all) reactions are thought to be reversible (Thauer, 2008).

Our analysis of the D-spiked water experiments, together with the D-labeled acetate experiment, suggests that up to 1.9 out of four hydrogen atoms in methane are derived from water-H. In addition to one hydrogen atom that is added at the last step of methanogenesis (the reduction of methyl-CoM, Figure 7 and 8), nearly another one of three hydrogen atoms in the methyl group of acetate could be exchanged with water. Since hydrogen isotope exchange between H_2O and CH_4 is sluggish, the exchange probably occurs at the CH_3-H_4SPT (methyl-tetrahydrosarcinaopterin) intermediate via H-abstraction to form CH_2=H_4SPT (the exchange can also occur at the methyl-CoM moiety, Scheller et al., 2013). This part of the pathway is not required for the acetoclastic metabolism but can occur as a side reaction. A similar D/H exchange mechanism was suggested to explain the observed scrambling of CD_3COO- during the incubation of methanogenic sediments (de Graaf et al., 1996). Because up to 0.9 out of three methyl-H atoms are exchanged, the flux of this side reaction is estimated to be at most 0.3 H (=0.9/3) per uptake of one acetate (Figure 8-A).

When deuterium-labeled acetate (CD_3COO^-) was used as a substrate, the major product (68%) was the isotopologue CD_3H. However, the isotopologues CD_2H_2, CDH_3 and CH_4 were also formed (Figure 4). Among the four isotopologues, the fraction of CH_4 isotopologues was disproportionally high. This is because CH_4 and non-deuterated acetate are carried over from the inoculum. If all CH_4 isotopologues are from the inoculum, the proportion of CD_3H isotopologues is 79% (=68/(5+13+68)) over CD_3H, CH_2D_2 and CH_3D isotopologues. This is the maximum fraction since a small quantity (most likely less than 5%) could be produced from CD_3COO^-. Following the model of D/H exchange at the CH_3-H_4SPT step as described above, this means that less than 100% yield of CD_3H is explained by the loss of CD_3-H_4SPT to CD_2=H_4SPT of 0.2 per one CD_3COO^-. The reaction from CD_3-H_4SPT to CD_2=H_4SPT and from CD_3-CoM to CD_3H would accompany deuterium isotope effects of $^2\alpha_p$ $^2\alpha_s^2$ and $^2\alpha_s^3$, respectively. Thus, the corresponding

flux for CH_3COO^- can be higher by the ratio of the two isotope effects ($^2\alpha_s/^2\alpha_p$), which could be as high as ~2 based on *in vitro* study of a similar reaction (≈0.84/0.41) (Scheller et al., 2013). Note that the medium water (and thus intercellular water) contain very little deuterium such that there is practically no back flux from CD_2=H_4SPT to CD_3-H_4SPT (Figure 8-B). Thus, H/D scrambling at the CH_3-moiety can be explained by the reverse flux of 0.2 to 0.3 based on the estimate from the D-spiked medium (0 to 0.3) and CD_3COO^- experiments (0.2 to ~0.4) (Figure 8).

4.4 Origin of ^{13}C-H signals in methane from acetoclastic methanogenesis

Measured $\Delta^{13}CH_3D$ values are -1.7 to -3.1, -1.1 to -3.8, -4.2 to -5.2‰ for *Methanosarcina* cultures grown on acetate, H_2+CO_2, and methanol, respectively, and are weakly correlated with δD_{H2O} of the medium (Figure 3B). The linear fit and standard error (95% confidence interval) was calculated following York et al. (2004). The slope ($\Delta^{13}CH_3D/\delta D$) for acetate is 0.0016±0.0012, hydrogen is 0.0020±0.0010 and methanol is 0.0019±0.0014. While this is a small sample size, these are statistically not zero. These anti-clumped $\Delta^{13}CH_3D$ values can originate from 1) mixing of two or more pools of methane or its precursor with different $\delta^{13}C$ and δD values, 2) transfer of the methyl-group of acetate and methanol with pre-existing anti-clumped signals (for acetate and methanol cultures), and/or 3) intrinsic kinetic isotope effects associated with enzymatic reactions common to three pathways, such as the reduction of methyl-CoM (Figure 7).

It has been well known that mixing is non-linear in the clumped isotope system such that mixing of two pools of methane yields a $\Delta^{13}CH_3D$ value that is not between the two $\Delta^{13}CH_3D$ values of original two reservoirs (Eiler and Schauble, 2004; Affek and Eiler, 2006; Affek et al., 2007; Defliese and Lohmann, 2015). When two pools of methane (A and B) are mixed, the $\Delta^{13}CH_3D$ value of the mixture (Δ_{mix}) can be approximated as:

$$\Delta_{mix} \approx (1\text{-}f)\,\Delta_A + f\Delta_B + f(1\text{-}f)\,(\delta^{13}C_A - \delta^{13}C_B)(\delta D_A - \delta D_B) \quad (28)$$

where *f* is the mixing ratio of pool B (Wang et al., 2015). The first and second terms show linear mixing between two $\Delta^{13}CH_3D$ values (Δ_A and Δ_B), whereas the third term produces a curvature following a quadratic function to *f*. This bias becomes the largest when the two pools of methane are mixed at a 1:1 ratio (i.e., *f*=0.5), and proportional to the product of the difference of δ values between the two pools of methane. Mixing of a ^{13}C- and D-enriched pool with a ^{13}C- and D-depleted pool would produce a positive (low temperature) bias, whereas diagonal mixing (e.g., mixing between a ^{13}C-enriched and a D-depleted pool with a ^{13}C-depleted and a D-enriched pool) would produce a negative (high temperature) bias in $\Delta^{13}CH_3D$. By extension, the mixing effect for doubly-deuterated clumped methane ($^{12}CH_2D_2$) will always produce a positive (low temperature) bias (Young et al., 2016). Equation (28) can be used to model reaction branching (i.e., producing

two products) or reversible reactions (where *mix* is the source and A and B are forward and backward reactions).

A fully quantitative model for the isotope systematics for the acetoclastic pathway in Figure 8 is the scope of future study, but equation (28) can be used to test the magnitude of any $\Delta^{13}CH_3D$ bias due to mixing. For example, mixing of two reservoirs (or fluxes) in equal portions (f=0.5) with $\delta^{13}C$ and δD differing by 40‰ and -300‰, respectively, can produce a non-linear bias of -3‰ (0.5(1-0.5)×0.04×(-0.3)). These magnitudes of kinetic ^{13}C- or D-isotope effects are possible. Therefore, an anti-clumped $\Delta^{13}CH_3D$ value of -3‰ can be produced entirely by mixing. For the acetoclastic cultures in these experiments, however, the value of $\Delta^{13}CH_3D$ was not sensitive to the δD value of the medium, which changed from -35 to 360‰ (Figure 3B), indicating that the mixing (between C-H bonds with water-derived H and methyl-derived H) is unlikely to be the major source of anti-clumped signals observed.

Calculations from the D-spiked cultures grown on acetate reported in this study showed that approximately up to two out of four hydrogen atoms in CH_4 are derived from water, while only one is required from stoichiometry. On average, the methyl group of acetate contributes 2 to 3 hydrogen atoms to one methane molecule, presumably also carrying its original ^{13}C-D signal. Although the degree of ^{13}C-D clumping of the methyl group of acetic acid (or methanol) cannot be measured by our current instrumentation, we expect its ^{13}C-D clumping signal is not much different from that of CH_4. This is because most industrial acetate (the likely source of sodium acetate used in this study) is produced from the high temperature (150 to 200°C) catalytic reaction of methanol and carbon monoxide (e.g., Eby and Singleton, 1983). Industrial methanol, in turn, is produced from carbon monoxide, carbon dioxide, and hydrogen at high temperature (typically 200 to 300°C) (Cheng and Kung, 1994). Based on theoretical calculations from modeled vibrational frequencies, Wang et al. (2015) reported that the *equilibrium* ^{13}C-D clumping of simple carbon compounds have a relatively narrow range of clumped isotope effects from +5.9 to +6.2‰ at 25°C for the molecules studied (methane, methanol, formaldehyde, formic acid, methanethiol, acetic acid). This indicates that the ^{13}C-D clumped isotope effect is not sensitive to detailed bonding environments. This is reasonable considering that the ^{13}C-D clumped isotope effect largely originates from a zero point energy shift (ΔZPE) associated with the C-H stretching vibration frequency at around 3000 cm^{-1}; bending vibration is much lower in energy (1350 cm^{-1}) and the ΔZPE is relatively small (Whitehill et al., 2017). Therefore, we estimate that the acetate or methanol may thus carry a $\Delta^{13}CH_3D$ signal of 1.6 to 3.1‰ assuming the near-equilibrium reaction between 150 and 300°C. If we assume that acetate was produced at the lower end of this temperature range (150°C) and methanol was produced at the higher end (300°C), this would correspond to equilibrium values of 3.1‰ for acetate vs. 1.6‰ for methanol. It is possible that this discrepancy could explain part, but not all of the difference between the $\Delta^{13}CH_3D$ values of the

acetoclastic and methylotrophic cultures. Nonetheless, experiments with various sources of acetic acid, natural and/or synthetic, will be needed to constrain the degree of non-equilibrium signals in ^{13}C-D bonds of acetic acids.

Another possibility is that the observed anti-clumped signal originates during the addition of the last hydrogen atom of methane. By applying equation (28), the $\Delta^{13}CH_3D$ value of methane (Δ_{CH4}) is expected to carry ¾ signal from methyl precursor (CH_3-CoM, Δ_{CH3}), and ¼ from the last H added:

$$\Delta_{CH4} = \frac{3}{4}(\ln \gamma_S + \Delta_{CH3}) + \frac{1}{4}\ln \gamma_P \qquad (29)$$

where γ_S and γ_P are kinetic clumped isotope effects for the secondary and primary D-addition (equations 13 and 14). Here, the non-linearity bias in equation (28) does not apply, because ^{13}C isotope effects for secondary and primary processes will be nearly identical (i.e., $\delta^{13}C_A - \delta^{13}C_B \simeq 0$).

What are the values of γ_S and γ_P? Applying transition state theory, Whitehill et al. (2017) presented a detailed analysis of the kinetic clumped effect for the gas phase oxidation of methane by the OH radical. We use their framework to make an approximate inference for this study. According to Whitehill et al. (2017), clumped isotope effects can be explained by the difference of zero-point energy shifts (ΔZPE) between $^{13}CH/^{12}CH$ and $^{13}CD/^{12}CD$. For methane, the ΔZPE for $^{13}CH_4$ vs. $^{12}CH_4$ is 29.8 cm^{-1} and that for $^{13}CH_3D$ vs. $^{12}CH_3D$ is 31.9 cm^{-1}. The difference between the two, ΔΔZPE of 2.1 cm^{-1}, is the origin of clumped effect (Whitehill et al., 2017). Transition state for the last step of methanogenesis involves a methyl radical intermediate with trigonal planar geometry (Scheller et al., 2013; Wongnate et all, 2017). We estimated the ΔΔZPE of the methyl radical of 2.1cm^{-1} using unrestricted MP2 with basis set aug-cc-pVQZ basis set. ΔΔZPE for reactant (CH_3-S-CoM, approximated by methylthiol, Wang et al., 2015) and transition state (approximated by the methyl radical) suggests that there is little kinetic clumped effect for the secondary reaction such that γ_S is expected to be close to unity. Whitehill et al. (2017) also showed that the imaginary frequency and tunneling terms do not produce clumped effects (within transition state theory), although the Wigner tunneling correction used in the study is highly approximated.

For the primary reaction, the C-D bond becomes loose at a transition state, contributing a smaller ΔΔZPE between 0 and 2.1 cm^{-1} (it is 0.5cm^{-1} for CH_3-D-OH transition state, Whitehill et al., 2017). For the bond forming reaction, ^{13}C-D is slightly preferred but not as much as equilibrium (γ_P<1.006). However, the anti-clumped effect (γ_P<1) is unlikely because it requires the ΔΔZPE to have the opposite sign (i.e., smaller ΔZPE for $^{13}CD/^{12}CD$ than $^{13}CH/^{12}CH$) at the transition state. Thus, based on this transition state model, γ_P could take any value between 1.000 and 1.006.

For example, if $\ln(\gamma_S)$ and Δ_{CH3} are 0.0 and 1.6 ‰, respectively, the value of $\ln(\gamma_P)$ of -13 ‰ is required to explain the observed $\Delta^{13}CH_3D$ value in the acetate culture of ~ -3‰ (equation (29). The magnitude of this kinetic anti-clumped effect has been implicated by Wang et al. (2015) as well as Stolper et al. (2015) to explain the observed values for natural samples. Low $\Delta^{13}CH_3D$ values for methanol cultures (-4.2 to -4.9 ‰) suggest that the methyl group of methanol may carry lower $\Delta^{13}CH_3D$ values.

Another possibility is that the anti-clumping effect for methanol cultures is related to the faster growth rate of methylotrophic compared to acetoclastic and hydrogenotrophic cultures. Cultures were incubated until they had produced enough methane for our analyses (>5mL, STP) which was reached over the course of different incubation times as noted in Table 2. Although exact experiment durations and methane concentrations were not controlled for in all experimental setups, incubation times and volume of methane produced are reported for Set 2 cultures (Table 2). Despite some measurement uncertainty, it appears methanol cultures generated methane more quickly. Quantifying the effect of growth rate warrants investigation in future work.

A series of studies suggest the potential importance of quantum mechanical tunneling in some H transfer reactions, in particular, during the oxidation of alcohol by dehydrogenase (Cha et al., 1989; Klinman and Kohen, 2013). Experimental evidence that supports tunneling includes the observed mass-independent fractionation among H/D/T, departure from the rule of geometric mean for multiply-deuterated (clumped) substrates, rate enhancement at low temperatures (Klinman and Kohen, 2013; Srinvasan et al., 1985; Amin et al., 1988; Huskey, 2007), and the anti-clumped CH_2D_2 abundance (Young et al., 2017). The large anti-clumped effect may be due to the tunneling effect, which is only approximated in the above transition state model. The test for this hypothesis would include *in vitro* enzyme assay experiments similar to Scheller et al. (2013), or high-level quantum mechanical modeling with accurate geometry and potential energy surface at the key transition state (e.g., Chen et al., 2012; Klinman and Kohen, 2013; Wongnate et al., 2016).

4.5 Non-equilibrium vs. equilibrium $\Delta^{13}CH_3D$ signals of methane in the environment

This study corroborates previous studies (Stolper et al., 2015; Wang et al., 2015; Douglas et al., 2016; Wang et al., 2016; Young et al., 2016; Young et al., 2017) and demonstrates that non-equilibrium (i.e., kinetic) clumped methane isotopologue signals are common for methane produced by microbial methanogenesis in laboratory cultures (Figure 1, Figure 9).

Our results are consistent with kinetic signals in methane sampled from freshwater environments (e.g. swamps and lakes), where acetoclastic methanogenesis, as opposed to hydrogenotropic methanogenesis, is thought to be the dominant source of methane (e.g., Conrad

2005; Ferry 2010). Nonetheless, our results demonstrate that low $\Delta^{13}CH_3D$ values are consistently out of equilibrium in batch culture and in environmental samples, but that this is not necessarily dependent on the metabolic pathway (hydrogenotrophic, methlyotrophic, or acetoclastic). Thus, $^{13}CH_3D$ isotopologue compositions cannot be used alone to resolve which methanogenic pathway is dominant in the environment.

Although dominantly microbial in origin, methane in marine environments (e.g. pore water and hydrate) tends to carry equilibrium or near-equilibrium $^{13}CH_3D$ abundances (Stolper et al., 2015; Wang et al., 2015). This is also corroborated by δD_{CH4} values that are relatively constant at -180±10‰ (e.g., Whiticar, 1999; Okumura et al., 2016), which is close to the expected value for methane in equilibrium with seawater water (with $\delta D \simeq 0$ ‰) (Horibe and Craig, 1995). It was suggested that "slow" methanogenesis under small thermodynamic drive (low environmental H_2 concentration) would produce near-equilibrium clumped isotopologue signals (Wang et al., 2015; Stolper et al., 2015). Oxidative cycles of methane also modify clumped isotopologue signals of environmental methane. The aerobic oxidation of methane by *Methylococcus*, for example, is characterized by kinetic clumped isotope effects ($\gamma \simeq 1$), and residual methane can exhibit strong non-equilibrium signals (Wang et al., 2016). In contrast, anaerobic oxidation of methane (AOM), thought to be the reverse process of methanogenesis (Hallam et al., 2004; Scheller et al., 2013; Wang et al., 2014), has been shown to operate with significant back-flux (Holler et al., 2011) and produce near-equilibrium carbon isotope fractionation (e.g., Yoshinaga et al., 2014). Methane cycling involving AOM and methanogenesis likely promotes near-equilibrium isotopologue distributions, in particular, in marine environments, and may contribute to near-equilibrium δD as well as $\Delta^{13}CH_3D$ signals. Conversely, bulk δD and $\Delta^{13}CH_3D$ values of methane may primarily reflect kinetic versus equilibrium signals and the rate of methanogenesis more so than metabolic pathways.

5. Conclusions

This study reports the $\Delta^{13}CH_3D$ systematics of microbial methane produced by pure cultures of methanogens. Our results show that the $\Delta^{13}CH_3D$ signals are not directly pathway dependent, as cultures of *M. barkeri* and *M. mazei* grown on acetate, methanol, and H_2+CO_2 all yield methane that is depleted in $^{13}CH_3D$, which seems to be characteristic of microbial methanogenesis in near-surface environments (lakes, swamps and ruminants). For mesophilic methanogens, the lowest $\Delta^{13}CH_3D$ values were produced for methane from cultures grown on methanol. Methanol cultures grew faster (incubation time of ~3 days) than those grown on acetate or H_2+CO_2 (incubation time of ~30 days). Thus, the $\Delta^{13}CH_3D$ values of methane may be related to the rate at which methane is produced rather than to the substrate used. Mesophilic methanogens

(*M. barkeri*) produced anti-clumped $\Delta^{13}CH_3D$ values (<0), while thermophilic and hyperthermophillic (*Methanothermococcus* and *Methanocaldococcus*) methanogens produced less kinetic signals.

Experiments with deuterated water or acetate aid in determining the source of hydrogen atoms in methane. The deuterated water experiments confirm that the four hydrogen atoms that form methane in hydrogenotrophic methanogenesis are derived from water. For the acetoclastic culture, 1.6 to 1.9 H atoms are derived from water, whereas only one is required by stoichiometry, suggesting some reversibility and isotope exchange at the methyl precursor. The deuterium spiked experiments also demonstrate that the observed non-equilibrium signals cannot be explained by the mixing of two pools of C-H bonds (e.g., from methyl group of acetate and one C-H bond formed during acetoclastic methanogenesis). The production of low $\Delta^{13}CH_3D$ values independent of the methanogenic pathway, suggests, although not exclusively, that the most of the kinetic signal is produced during the enzymatic reactions common in the three methanogenic pathways, such as the reduction of methyl-coenzyme M.

Acknowledgements:
We thank H. Taubner, J. Wendt, X. Prieto, S. Burns, A. Colman, and G. Olack for technical assistance and $\delta^{13}C$ and δD measurements. We also thank Alex Sessions, Shinsuke Kawagucci, one anonymous reviewer, and the associate editor, Ed Hornibrook, for constructive feedback. Grants from the National Science Foundation (EAR-1250394 to S.O.), N. Braunsdorf and D. Smit of Shell PTI/EG (to S.O.), the Deep Carbon Observatory (to S.O., M.K., K.-U.H., D.S.G.), the Gottfried Wilhelm Leibniz Program of the Deutsche Forschungsgemeinschaft (HI 616-14-1 to K.-U.H.), and the Heisenberg Program (KO3651-3-1 to M.K.) of the Deutsche Forschungsgemeinschaft supported this study. D.S.G. was also supported by a National Science Foundation Graduate Research Fellowship, the Neil and Anna Rasmussen Foundation Fund, the Grayce B. Kerr Fellowship, and a Shell-MIT Energy Initiative Graduate Fellowship. D.T.W. was supported by a National Defense Science and Engineering Graduate Fellowship. L.C.S. was supported by a NASA Earth and Space Science Fellowship (grant NNX11AP78H).

References

Affek H. P. and Eiler J. M. (2006) Abundance of mass $^{47}CO_2$ in urban air, car exhaust, and human breath. *Geochim. Cosmochim. Acta* **70**, 1–12.

Affek H. P., Xu X. and Eiler J. M. (2007) Seasonal and diurnal variations of $^{13}C^{18}O^{16}O$ in air: Initial observations from Pasadena, CA. *Geochim. Cosmochim. Acta* **71**, 5033–5043.

Alperin M. J. and Blair N. E. (1992) Factors that control the stable carbon isotopic composition of methane produced in an anoxic marine sediment. *Global Biogeochem. Cycles* **6**, 271–291.

Amin, M., Price, R.C. and Saunders, W.H. (1988) Isotope effects on isotope effects. Failure of the rule of the geometric mean as evidence for tunneling. Journal of the American Chemical Society 110, 4085-4086.

Balch W. E., Fox G. E., Magrum L. J., Woese C. R. and Wolfe R. S. (1979) Methanogens: Reevaluation of a unique biological group. *Microbiol. Rev.* **43**, 260-296.

Bapteste E., Brochier C. and Boucher Y. (2005) Higher-level classification of the Archaea: evolution of methanogenesis and methanogens. *Archaea* **1**, 353–363.

Bigeleisen J. and Mayer (1947) Calculation of equilibrium constants for isotopic exchange reactions. *J. Chem. Phys.* **15**, 261–267.

Blair N. E. and Carter W. D. (1992) The carbon isotope biogeochemistry of acetate from a methanogenic marine sediment. *Geochim. Cosmochim. Acta* **56**, 1247–1258.

Blaser M. and Conrad R. (2016) Stable carbon isotope fractionation as tracer of carbon cycling in anoxic soil ecosystems. *Curr. Opin. Biotechnol.* **41**, 122–129.

Burke R. A. (1993) Possible influence of hydrogen concentration on microbial methane stable hydrogen isotopic composition. *Chemosphere* **26**, 55–67.

Cha Y., Murray, C. and Klinman, J. (1989) Hydrogen tunneling in enzyme reactions. *Science* **243**, 1325-1330.

Chen S. L., Blomberg M. R. A. and Siegbahn P. E. M. (2012) How is methane formed and oxidized reversibly when catalyzed by Ni-containing methyl-coenzyme M reductase? *Chem. - A Eur. J.* **18**, 6309–6315.

Cheng, W.-H. and Kung, H.H. (1994) Methanol production and use. Marcel Dekker, New York.

Conrad R. (2005) Quantification of methanogenic pathways using stable carbon isotopic signatures: a review and a proposal. *Org. Geochem.* **36**, 739–752.

Conrad R., Claus P. and Casper P. (2009) Characterization of stable isotope fractionation during methane production in the sediment of a eutrophic lake, Lake Dagow, Germany. **54**, 457–471.

Coplen T. B. (2011) Guidelines and recommended terms for expression of stable-isotope-ratio and gas-ratio measurement results. *Rapid Commun. Mass Spectrom.* **25**, 2538–2560.

Daniels L., Fulton, G., Spencer, R. and Orme-Johnson, W. (1980) Origin of hydrogen in methane produced by Methanobacterium thermoautotrophicum. *J. Bacteriol* **141**, 694-698.

Defliese W. F. and Lohmann K. C. (2015) Non-linear mixing effects on mass-47 CO_2 clumped isotope thermometry: Patterns and implications. *Rapid Commun. Mass Spectrom.* **29**, 901–9.

Douglas P. M. J., Stolper D. A., Smith D. A., Walter Anthony K. M., Paull C. K., Dallimore S., Wik M., Crill P. M., Winterdahl M., Eiler J. M. and Sessions A. L. (2016) Diverse origins of Arctic and Subarctic methane point source emissions identified with multiply-substituted isotopologues. *Geochim. Cosmochim. Acta* **188**, 163–188.

Douglas P. M. J., Stolper D. A., Eiler J. M., Sessions A. L., Lawson M., Shuai Y., Bishop A., Podlaha O. G., Ferreira A. A., Santos Neto E. V., Niemann M., Steen A. S., Huang L.,

Chimiak L., Valentine D. L., Fiebig J., Luhmann A. J., Seyfried W. E., Etiope G., Schoell M., Inskeep W. P., Moran J. J. and Kitchen N. (2017) Methane clumped isotopes: Progress and potential for a new isotopic tracer. *Org. Geochem.* **113**, 262–282.

Eby R. T. and Singleton T. C. (1983) Chapter 10: Methanol Carbonylation to Acetic Acid. In *Applied Industrial Catalysis* (ed. B. E. Leach). Academic Press. p. 275.

Eiler J. M. (2007) "Clumped-isotope" geochemistry—The study of naturally-occurring, multiply-substituted isotopologues. *Earth Planet. Sci. Lett.* **262**, 309–327.

Eiler J. M. (2013) The isotopic anatomies of molecules and minerals. *Annu. Rev. Earth Planet. Sci.* **41**, 411–441.

Eiler J. M. and Schauble E. (2004) $^{18}O^{13}C^{16}O$ in Earth's atmosphere. *Geochim. Cosmochim. Acta* **68**, 4767–4777.

Ermler U., Grabarse W., Shima S., Goubeaud M. and Thauer R. K. (1997) Crystal structure of methyl coenzyme M reductase: The key enzyme of biological methane formation. *Science* **278**, 1457–1462.

Farquhar J., Johnston D. T. and Wing B. A. (2007) Implications of conservation of mass effects on mass-dependent isotope fractionations: Influence of network structure on sulfur isotope phase space of dissimilatory sulfate reduction. *Geochim. Cosmochim. Acta* **71**, 5862–5875.

Ferry J. G. (2010) How to make a living by exhaling methane. *Annu. Rev. Microbiol.* **64**, 453–473.

Grabarse W., Mahlert F., Shima S., Thauer R. K. and Ermler U. (2000) Comparison of three methyl-coenzyme M reductases from phylogenetically distant organisms: Unusual amino acid modification, conservation and adaptation. *J. Mol. Biol.* **303**, 329–344.

Hallam S. J., Putnam N., Preston C. M., Detter J. C., Rokhsar D., Richardson P. M. and DeLong E. F. (2004) Reverse methanogenesis: Testing the hypothesis with environmental genomics. *Science* **305**, 1457–1462.

Hartmann G. C., Santamaria E., Fernandez V. M., and Thauer R. K. (1996) Studies on the catalytic mechanism of H_2-forming methylenetetrahydromethanopterin dehydrogenase: Paraortho H_2 conversion rates in H_2O and D_2O. *J. Biol. Inorg. Chem.* **1**(5), 446–450.

Heuer V., Elvert M., Tille S., Krummen M., Mollar X. P., Hmelo L. R. and Hinrichs K.-U. (2006) Online $\delta^{13}C$ analysis of volatile fatty acids in sediment/porewater systems by liquid chromatography-isotope ratio mass spectrometry. *Limnol. Oceanogr. Methods*, 346–357.

Holler T., Wegener G., Niemann H., Ferdelman T. G., Boetius A., Kristiansen T. Z., Molina H., Pandey A., Werner J. K., Juluri K. R., Xu Y., Glenn D., Parang K. and Snyder S. H. (2012) Correction for Holler et al., Carbon and sulfur back flux during anaerobic microbial oxidation of methane and coupled sulfate reduction. *Proc. Natl. Acad. Sci.* **109**, 21170–21170.

Huskey, W.P. (2007) Multiple-Isotope Probes of Hydrogen Tunneling, Hydrogen-Transfer Reactions. Wiley-VCH Verlag GmbH & Co. KGaA, pp. 1285-1309.

Huber H., Thomm M., König H., Thies G., and Stetter K.O. (1982) *Methanococcus thermolithotrophicus*, a novel thermophilic lithotrophic methanogen. *Arch. Microbiol.* **132,** 47-50.

Hut G. (1987) Consultants' group meeting on stable isotope reference samples for geochemical and hydrological investigations. *Rep. to Dir. Gen.*, 16–18.

Inagaki F., Hinrichs, K.-U., Kubo Y., Bowles M. W., Heuer V. B., Ijiri A., Imachi H., Ito M., Kaneko M., Lever M. A., Morita S., Morono Y., Tanikawa W., Bihan M., Bowden S. A., Elvert M., Glombitza C., Gross D., Harrington G. J., Hori T., Li K., Limmer D., Murayama M., Ohkouchi N., Ono S., Purkey M., Sanada Y., Sauvage J., Snyder G., Takano Y.,

Tasumi E., Terada T., Tomaru H., Wang D. T. and Yamada Y. (2015) Exploring deep microbial life in coal-bearing sediment down to ~2.5 km below the ocean floor. *Science* **349**, 420–424.

Jones W., Leigh J., Mayer F., Woese C., Wolfe R. (1983) *Methanococcus jannaschii* sp. nov., an extremely thermophilic methanogen from a submarine hydrothermal vent. *Arch. Microbiol.* **136**, 254–261.

Kawagucci S., Kobayashi M., Hattori S., Yamada K., Ueno Y., Takai K. and Yoshida N. (2014) Hydrogen isotope systematics among H_2–H_2O–CH_4 during the growth of the hydrogenotrophic methanogen *Methanothermobacter thermautotrophicus* strain ΔH. *Geochim. Cosmochim. Acta* **142**, 601–614.

Klapp S. a., Bohrmann G., Kuhs W. F., Mangir Murshed M., Pape T., Klein H., Techmer K. S., Heeschen K. U. and Abegg F. (2010) Microstructures of structure I and II gas hydrates from the Gulf of Mexico. *Mar. Pet. Geol.* **27**, 116–125.

Klein A. R. and Thauer R. K. (1995) *Re*-face specificity at C14a of methylenetetrahydromethanopterin and *Si*-face specificity at C5 of coenzyme F_{420} for coenzyme F_{420}-dependent methylenetetrahydromethanopterin dehydrogenase from methanogenic archaea. *Eur. J. Biochem*. **227** (1–2), 169–174. K

Klein A. R., Fernandez V. M., and Thauer R. K. (1995a) H_2-forming N^5,N^{10}-methylenetetrahydromethanopterin dehydrogenase: Mechanism of H_2 formation analyzed using hydrogen isotopes. *FEBS Lett.* **368** (2), 203–206.

Klein A. R., Hartmann G. C., and Thauer R. K. (1995b) Hydrogen isotope effects in the reactions catalyzed by H_2-forming N^5, N^{10}-methylenetetrahydromethanopterin dehydrogenase from methanogenic archaea. *Eur. J. Biochem.* **233** (1), 372–376.

Klinman J. P. and Kohen A. (2013) Hydrogen tunneling links protein dynamics to enzyme catalysis. *Annu. Rev. Biochem.* **82**, 471–496.

Kung, Harold H & Cheng, Wu-Hsun, 1954- (1994). *Methanol production and use*. M. Dekker, New York

Kvenvolden K. A. (1993) Gas hydrates-geological perspective and global change. *Rev. Geophys.* **31**, 173–187.

Liu Q. and Liu Y. (2016) Clumped-isotope signatures at equilibrium of CH_4, NH_3, H_2O, H_2S and SO_2. *Geochim. Cosmochim. Acta* **175**, 252–270.

Lopes J. C., de Matos L. F., Harper M. T., Giallongo F., Oh J., Gruen D., Ono S., Kindermann M., Duval S. and Hristov A. N. (2016) Effect of 3-nitrooxypropanol on methane and hydrogen emissions, methane isotopic signature, and ruminal fermentation in dairy cows. *J. Dairy Sci.* **99**, 5335–5344.

Ma Q., Wu S. and Tang Y. (2008) Formation and abundance of doubly-substituted methane isotopologues ($^{13}CH_3D$) in natural gas systems. *Geochim. Cosmochim. Acta* **72**, 5446–5456.

McCalley C. K., Woodcroft B. J., Hodgkins S. B., Wehr R. a., Kim E.-H., Mondav R., Crill P. M., Chanton J. P., Rich V. I., Tyson G. W. and Saleska S. R. (2014) Methane dynamics regulated by microbial community response to permafrost thaw. *Nature* **514**, 478–481.

Okumura T., Kawagucci S., Saito Y., Matsui Y., Takai K. and Imachi H. (2016) Hydrogen and carbon isotope systematics in hydrogenotrophic methanogenesis under H_2-limited and H_2-enriched conditions: implications for the origin of methane and its isotopic diagnosis. *Prog. Earth Planet. Sci.* **3**, 14.

Ono S., Wang D. T., Gruen D. S., Sherwood Lollar B., Zahniser M. S., McManus B. J. and Nelson D. D. (2014) Measurement of a doubly substituted methane isotopologue, $^{13}CH_3D$, by Tunable Infrared Laser Direct Absorption Spectroscopy. *Anal. Chem.* **86**, 6487–6494.

Penger J., Conrad R. and Blaser M. (2012) Stable carbon isotope fractionation by methylotrophic methanogenic archaea. *Appl. Environ. Microbiol.* **78**, 7596–602.

Piasecki A., Sessions A., Lawson M., Ferreira A. A., Neto E. V. S. and Eiler J. M. (2016) Analysis of the site-specific carbon isotope composition of propane by gas source isotope ratio mass spectrometer. *Geochim. Cosmochim. Acta* **188**, 58–72.

Piasecki A., Sessions A., Peterson B. and Eiler J. (2016) Prediction of equilibrium distributions of isotopologues for methane, ethane and propane using density functional theory. *Geochim. Cosmochim. Acta* **190**, 1–12.

Pine M. J. and Barker H. A. (1956) Studies on the methane fermentation. XII. The pathway of hydrogen in the acetate fermentation. *J. Bacteriol.* **71**, 644–8.

Rees C. E. (1973) A steady-state model for sulphur isotope fractionation in bacterial reduction processes. *Geochim. Cosmochim. Acta* **37**, 1141–1162.

Reeves E. P., Seewald J. S. and Sylva S. P. (2012) Hydrogen isotope exchange between n-alkanes and water under hydrothermal conditions. *Geochim. Cosmochim. Acta* **77**, 582–599.

Riedel, M., Collett, T.S., Malone, MJ., and Expedition 311 Scientists (2006) *Proceedings of the IODP Integrated Ocean Drilling Program* **311**, Integrated Ocean Drill. Program, College Station, Tex.

Röckmann T., Popa M. E., Krol M. C. and Hofmann M. E. G. (2016) Statistical clumped isotope signatures. *Sci. Rep.* **6**, 31947.

Scheller S., Goenrich M., Thauer R. K. and Jaun B. (2013) Methyl-coenzyme M reductase from methanogenic archaea: Isotope effects on the formation and anaerobic oxidation of methane. *J. Am. Chem. Soc.* **135**, 14975-14984.

Schleucher J., Griesinger C., Schworer B., and Thauer R. K. (1994) H_2-forming N5,N10-methylenetetrahydromethanopterin dehydrogenase from *Methanobacterium thermoautotrophicum* catalyzes a ste- reoselective hydride transfer as determined by 2-dimensional NMR- spectroscopy. *Biochemistry* **33** (13), 3986–3993.

Schoell M. (1980) The hydrogen and carbon isotopic composition of methane from natural gases of various origins. *Geochim. Cosmochim. Acta* **44**, 649–661.

Schworer B., Fernandez V. M., Zirngibl C., and Thauer R. K. (1993) H_2-forming N^5, N^{10}-methylenetetrahydromethanopterin dehydrogenase from *Methanobacterium thermoautotrophicum*: Studies of the catalytic mechanism of H_2 formation using hydrogen isotopes. *Eur. J. Biochem*. **212** (1), 255–261.

Sessions A. L. and Hayes J. M. (2005) Calculation of hydrogen isotopic fractionations in biogeochemical systems. *Geochim. Cosmochim. Acta* **69**, 593–597.

Sim M. S., Ono S., Donovan K., Templer S. P. and Bosak T. (2011) Effect of electron donors on the fractionation of sulfur isotopes by a marine Desulfovibrio sp. *Geochim. Cosmochim. Acta* **75**, 4244–4259.

Srinivasan, R. and Fisher, H.F. (1985) Deuterium isotope effects for the nonenzymic and glutamate dehydrogenase catalyzed reduction of an α-imino acid by NADH. *J. Am. Chem. Soc.* **107**, 4301-4305.

Stewart L. C., Jung J., Kim Y., Kwon S., Park C., Holden J. F. and Holden J. F. (2015) *Methanocaldococcus bathoardescens* sp. nov., a hyperthermophilic methanogen isolated

from a volcanically active deep-sea hydrothermal vent. *Int. J. Syst. Evol. Microbiol.* **65,** 1280-1283.

Stolper D. A., Lawson M., Davis C. L., Ferreira A. A., Neto E. V. S., Ellis G. S., Lewan M. D., Martini A. M., Tang Y., Schoell M., Sessions A. L. and Eiler J. M. (2014) Formation temperatures of thermogenic and biogenic methane. *Science* **344**, 1500–1503.

Stolper D. A., Martini A. M., Clog M., Douglas P. M., Shusta S. S., Valentine D. L., Sessions A. L. and Eiler J. M. (2015) Distinguishing and understanding thermogenic and biogenic sources of methane using multiply substituted isotopologues. *Geochim. Cosmochim. Acta* **161**, 219–247.

Stolper D. A., Sessions A. L., Ferreira A. A., Santos Neto E. V., Schimmelmann A., Shusta S. S., Valentine D. L. and Eiler J. M. (2013) Combined ^{13}C–D and D–D clumping in methane: Methods and preliminary results. *Geochim. Cosmochim. Acta* **126**, 169–191.

Sugimoto A. and Wada E. (1995) Hydrogen isotopic composition of bacterial methane: CO_2/H_2 reduction and acetate fermentation. **59**, 1329–1337.

Thauer R. K. (1998) Biochemistry of methanogenesis: a tribute to Marjory Stephenson. *Microbiology* **144**, 2377–406.

Thauer R. K., Kaster A.-K., Seedorf H., Buckel W. and Hedderich R. (2008) Methanogenic archaea: ecologically relevant differences in energy conservation. *Nat. Rev. Microbiol.* **6**, 579–91.

Urey H. C. (1947) The thermodynamic properties of isotopic substances. *J. Chem. Soc.*, 562.

Vanwonterghem I., Evans P. N., Parks D. H., Jensen P. D., Woodcroft B. J., Hugenholtz P. and Tyson G. W. (2016) Methylotrophic methanogenesis discovered in the archaeal phylum Verstraetearchaeota. *Nat. Microbiol.* **1**, 16170.

Valentine D. L., Chidthaisong A., Rice A., Reeburgh W. S. and Tyler S. C. (2004) Carbon and hydrogen isotope fractionation by moderately thermophilic methanogens. *Geochim. Cosmochim. Acta* **68**, 1571–1590.

Wagner T., Kahnt J., Ermler U. and Shima S. (2016) Didehydroaspartate Modification in Methyl-Coenzyme M Reductase Catalyzing Methane Formation. *Angew. Chemie - Int. Ed.* **55**, 10630–10633.

Waldron, S., Lansdown, J., Scott, E., Fallick, A. and Hall, A. (1999) The global influence of the hydrogen isotope composition of water on that of bacteriogenic methane from shallow freshwater environments. *Geochim. Cosmochim. Acta* **63**, 2237-2245.

Wang D. T., Gruen D. S., Lollar B. S., Hinrichs K., Stewart L. C., Holden J. F., Hristov A. N., Pohlman J. W., Morrill P. L., Könneke M., Delwiche K. B. and Reeves E. P. (2015) Nonequilibrium clumped isotope signals in microbial methane. *Science* **348**, 428–431.

Wang D. T., Welander P. V. and Ono S. (2016) Fractionation of the methane isotopologues $^{13}CH_4$, $^{12}CH_3D$, and $^{13}CH_3D$ during aerobic oxidation of methane by *Methylococcus capsulatus* (Bath). *Geochim. Cosmochim. Acta* **192**, 186–202.

Wang F.-P., Zhang Y., Chen Y., He Y., Qi J., Hinrichs K.-U., Zhang X.-X., Xiao X. and Boon N. (2014) Methanotrophic archaea possessing diverging methane-oxidizing and electron-transporting pathways. *ISME J.* **8**, 1069–1078.

Webster C. R., Mahaffy P. R., Atreya S. K., Flesch G. J., Mischna M. A., Meslin P.-Y., Farley K. A., Conrad P. G., Christensen L. E., Pavlov A. A., Martin-Torres J., Zorzano M.-P., McConnochie T. H., Owen T., Eigenbrode J. L., Glavin D. P., Steele A., Malespin C. A., Archer P. D., Sutter B., Coll P., Freissinet C., McKay C. P., Moores J. E., Schwenzer S.

P., Bridges J. C., Navarro-Gonzalez R., Gellert R. and Lemmon M. T. (2015) Mars methane detection and variability at Gale crater. *Science* **347**, 415–417.

Wecht K. J., Jacob D. J., Frankenberg C., Jiang Z. and Blake D. R. (2014) Mapping of North American methane emissions with high spatial resolution by inversion of SCIAMACHY satellite data. *J. Geophys. Res. Atmos.* **119**, 7741–7756.

Whitehill A. R., Joelsson L. M. T., Schmidt J. A., Wang D. T., Johnson M. S. and Ono S. (2017) Clumped isotope effects during OH and Cl oxidation of methane. *Geochim. Cosmochim. Acta* **196**, 307–325.

Whiticar M. (1990) A geochemial perspective of natural gas and atmospheric methane. *Org. Geochem.* **16**, 531–547.

Whiticar M. J. (1999) Carbon and hydrogen isotope systematics of bacterial formation and oxidation of methane. *Chem. Geol.* **161**, 291–314.

Yeung L. Y. (2016) Combinatorial effects on clumped isotopes and their significance in biogeochemistry. *Geochim. Cosmochim. Acta* **172**, 22–38.

Yoshinaga M. Y., Holler T., Goldhammer T., Wegener G., Pohlman J. W., Brunner B., Kuypers M. M. M., Hinrichs K.-U. and Elvert M. (2014) Carbon isotope equilibration during sulphate-limited anaerobic oxidation of methane. *Nat. Geosci*. **7**, 190–194.

Yoshioka H., Sakata S. and Kamagata Y. (2008) Hydrogen isotope fractionation by *Methanothermobacter* thermoautotrophicus in coculture and pure culture conditions. *Geochim. Cosmochim. Acta* **72**, 2687–2694.

York D., Evensen, N.M., Martınez, M.L. and Delgado, J.D.B. (2004) Unified equations for the slope, intercept, and standard errors of the best straight line. *Am. J. Phys.* **72**, 367-375.

Young E. D., Rumble D., Freedman P. and Mills M. (2016) A large-radius high-mass-resolution multiple-collector isotope ratio mass spectrometer for analysis of rare isotopologues of O_2, N_2, CH_4 and other gases. *Int. J. Mass Spectrom.* **401**, 1–10.

Young E. D., Kohl I. E., Lollar B. S., Etiope G., Rumble D., Li S., Haghnegahdar M. a., Schauble E. a., McCain K. A., Foustoukos D. I., Sutclife C., Warr O., Ballentine C. J., Onstott T. C., Hosgormez H., Neubeck A., Marques J. M., Pérez-Rodríguez I., Rowe A. R., LaRowe D. E., Magnabosco C., Yeung L. Y., Ash J. L. and Bryndzia L. T. (2017) The relative abundances of resolved $^{12}CH_2D_2$ and $^{13}CH_3D$ and mechanisms controlling isotopic bond ordering in abiotic and biotic methane gases. *Geochim. Cosmochim. Acta* **203**, 235–264.

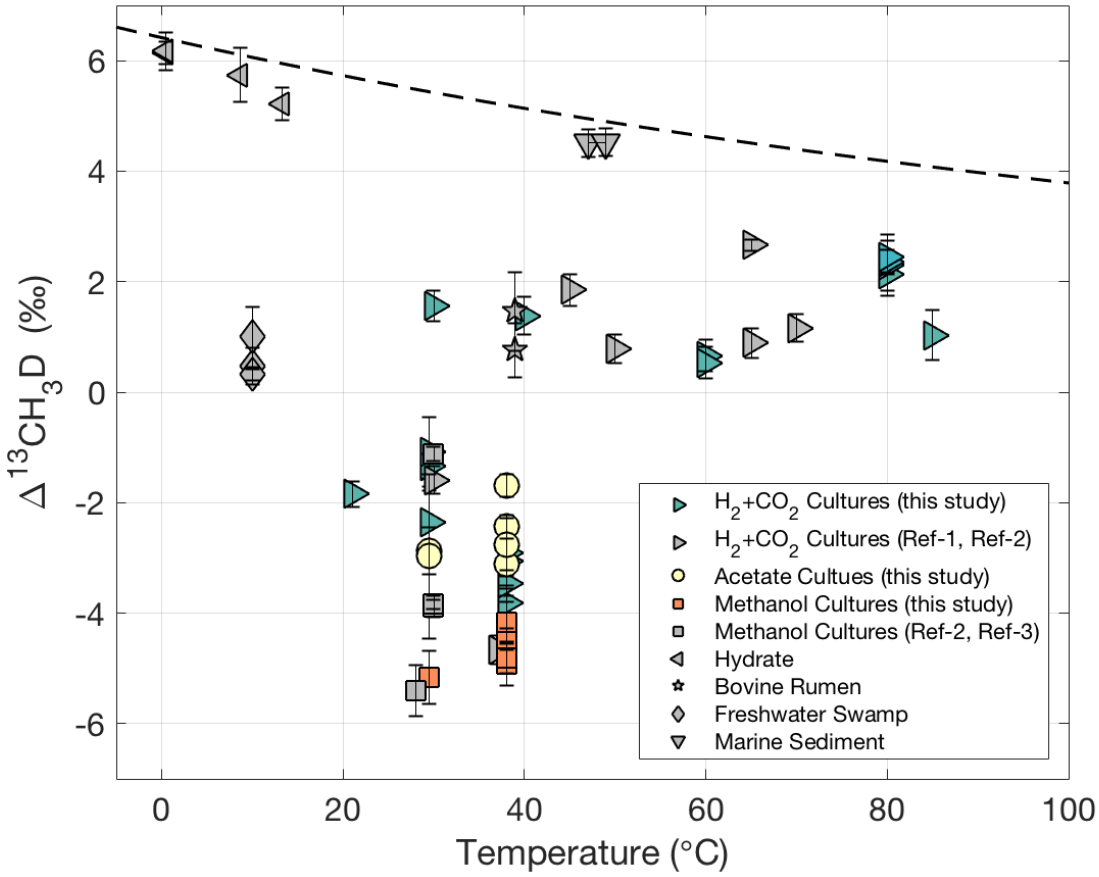

Figure 1. Clumped methane, $\Delta^{13}CH_3D$, plotted against environmental temperatures. The dashed line represents the equilibrium $\Delta^{13}CH_3D$ values calibrated experimentally using heated methane calibrations between 400 and 150°C (Ono et al., 2014; Wang et al., 2015) and extrapolated for lower temperatures. Colored triangles, circles, and squares represent laboratory cultures from this study. Right-facing triangles refer to H_2+CO_2 cultures, circles to acetate cultures and squares to methanol cultures. A subset of samples was previously published in Wang et. (2015) as noted in Table 2. For comparison to this work, previously reported H_2+CO_2 and methanol cultures from Stolper et al., 2014 (Ref-1), Young et al., 2017 (Ref-2) and Douglas et al., 2016 (Ref-3) are plotted with grey symbols which correspond to the substrate used. Also plotted are environmental methane samples reported in Wang et al. (2015) (Grey symbols). Bovine rumen samples are published in Lopes et al. (2016). In situ temperatures for hydrate samples are calculated using depths and geothermal gradients listed in IODP reports (Riedel et al., 2006). All previously published culture data are reported according to their original measurement notation ($\Delta^{13}CH_3D$ or $\Delta18$).

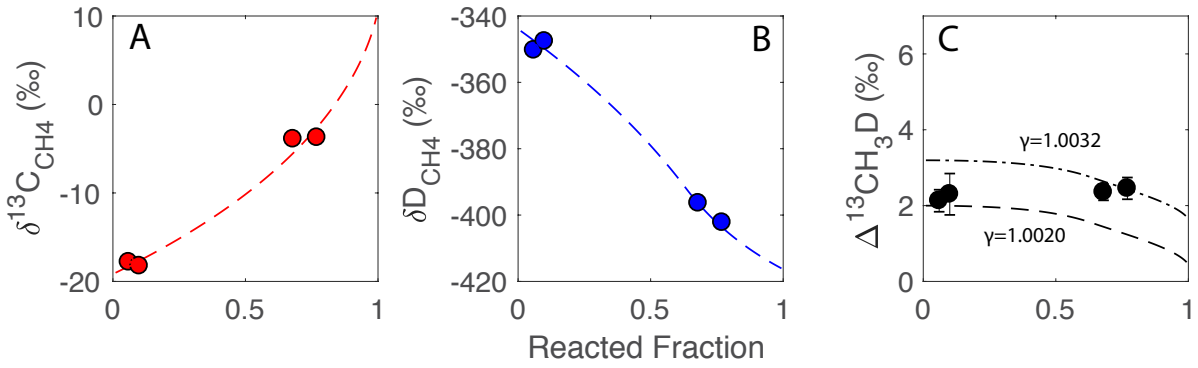

Figure 2. Isotope systematics of $\delta^{13}C$, δD, $\Delta^{13}CH_3D$ over the course of a batch culture experiment. Hydrogenotrophic methanogens (*Methanocaldococcus bathoardescens*) grown at 80°C. Reacted fraction refers to the fraction of carbon dioxide converted to methane. The filled circles represent methane measured from culture experiments. The dashed lines show the results of a closed system model discussed in section 4.1. $\delta^{13}C$, δD and $\Delta^{13}CH_3D$ of methane are shown in A, B, and C, respectively. Results for two γ values are shown in C. See text for other fractionation factors. The $\delta^{13}C$ value of initial CO_2 was fitted to 10.9‰.

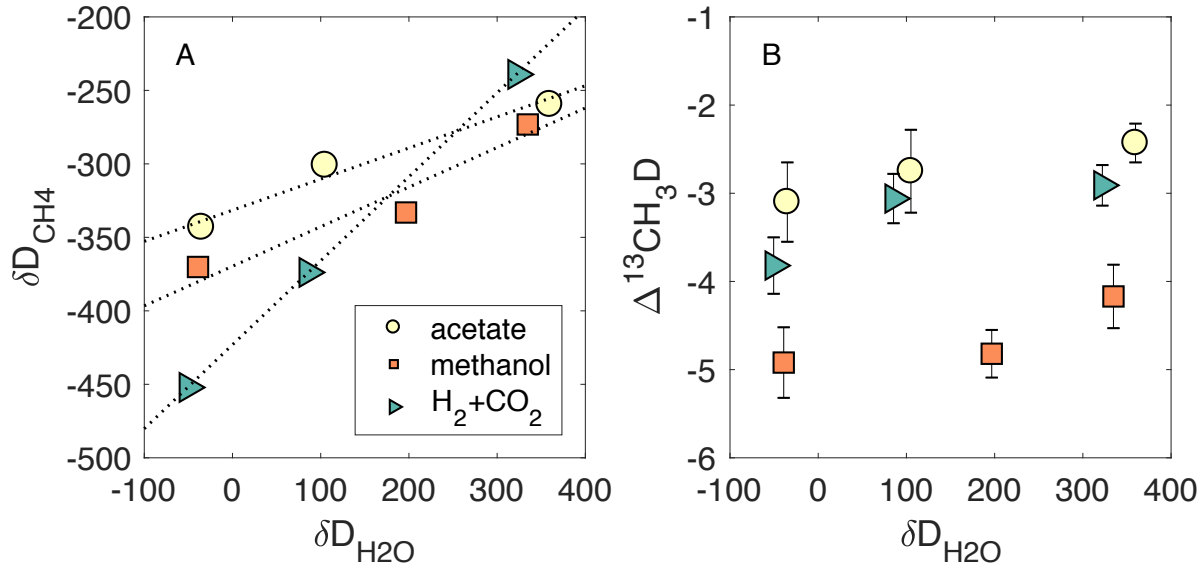

Figure 3. The δD and $\Delta^{13}CH_3D$ values of methane produced by *M. barkeri* in deuterium-spiked medium. Cultures were grown at 38°C, and isotopic compositions of methane are compared against δD values of media water in D-spiked experiments. Includes Set 2 data.

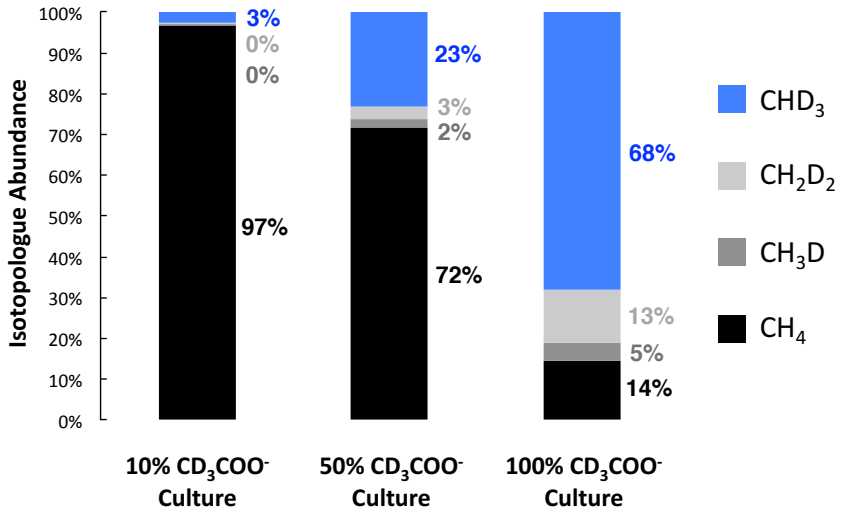

Figure 4. Relative isotopologue abundances of methane produced by *M. barkeri* in batch cultures spiked with CD_3COO^- (10, 50, 100%). Isotopologue composition was determined by FTIR, and relative abundances of methane-d_n isotopologues were calibrated against high-purity synthetic standards. CD_4 was not detected in any of the experiments.

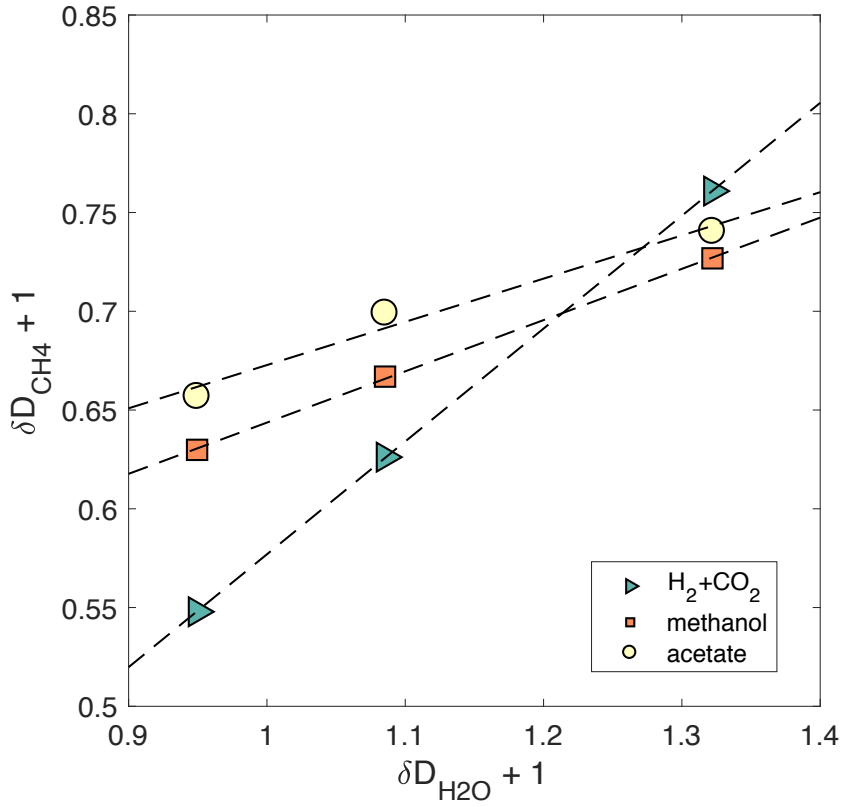

Figure 5. The hydrogen isotope composition of microbial methane vs. the deuterium composition of media water in spiked culture experiments. *M. barkeri* grown on three different substrates. In comparison to Figure 3A, the axes in this figure are plotted as δD + 1 to take into account the non-linearity in δD.

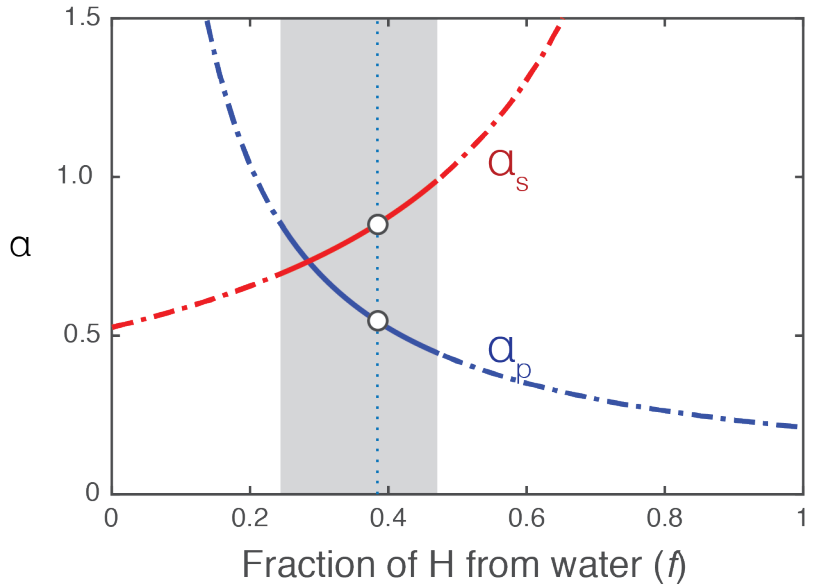

Figure 6. The fractionation factor (α) as a function of the fraction of hydrogen derived from water (*f*) in acetoclastic methanogenesis in D_2O spiked water experiments. Grey shading indicates the range of *f* values that satisfy α_p and α_s <1 and 0.25<*f*<1. The dashed vertical line and open circles correspond to the solution when $\alpha_s = 0.85$.

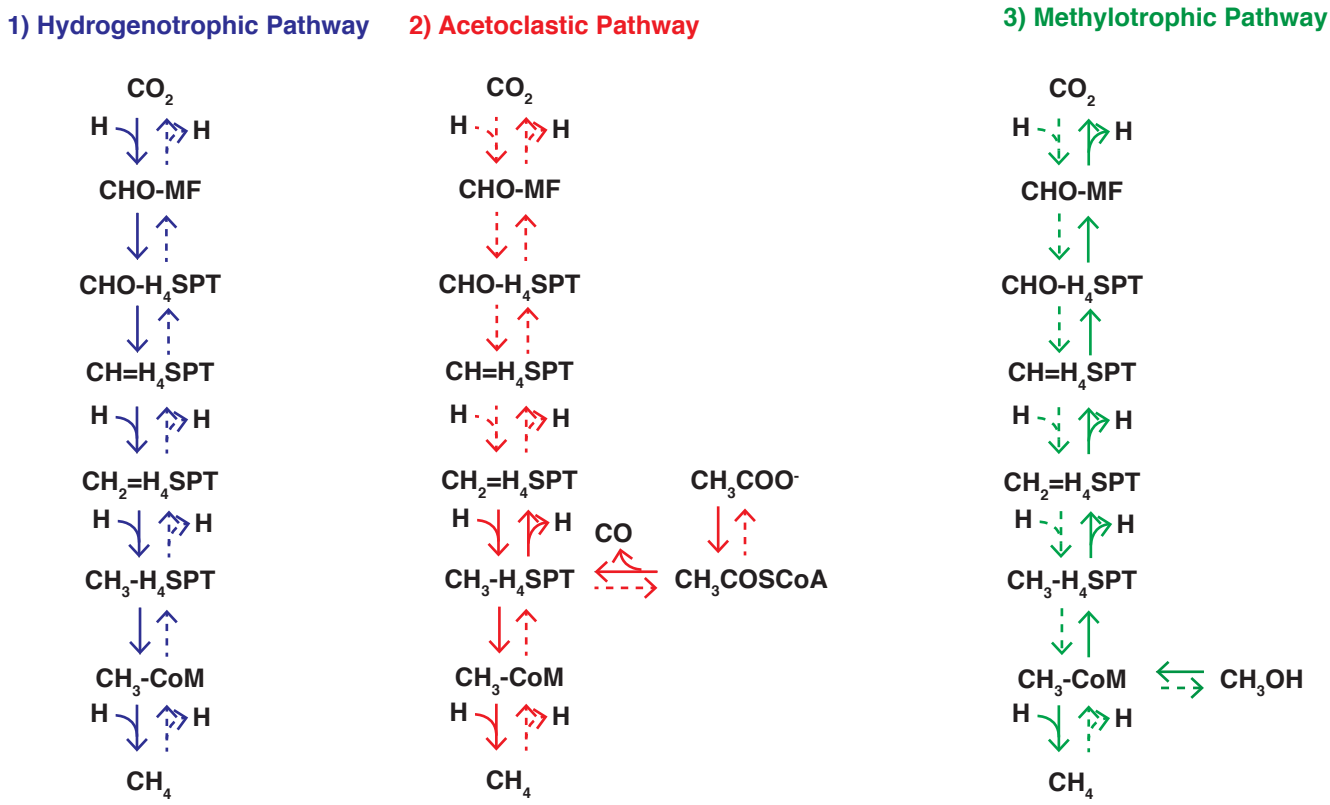

Figure 7: Three methanogenic pathways for *Methanosarcina*. The solid arrows represent the predominant direction of the reaction, and the dashed arrows represent the backward reaction, which is thought to be minor. Two solid arrows are used to indicate that the reactions are thought to be reversible, according to the literature, not specifically evaluated in this study. In the hydrogenotrophic pathway (blue), CO_2 is reduced by a series of four two-electron processes, each adding one H atom. C_1 compounds are carried with cofactors (MF, methanofuran, H_4SPT, tetrahydrosarcinaopterin, CoM, coenzyme M). For the acetoclastic pathway, acetate is first activated by acetyl co-A (via acetyl phosphate), acetyl co-A is split to methyl (CH_3-) and a carbonyl moiety (CO), and the latter is oxidized to CO_2. The methylotrophic pathway is overall a disproportionation reaction in which one methyl group is oxidized to CO_2 via a reversed methanogenic pathway, and three additional methyl groups are reduced to methane.

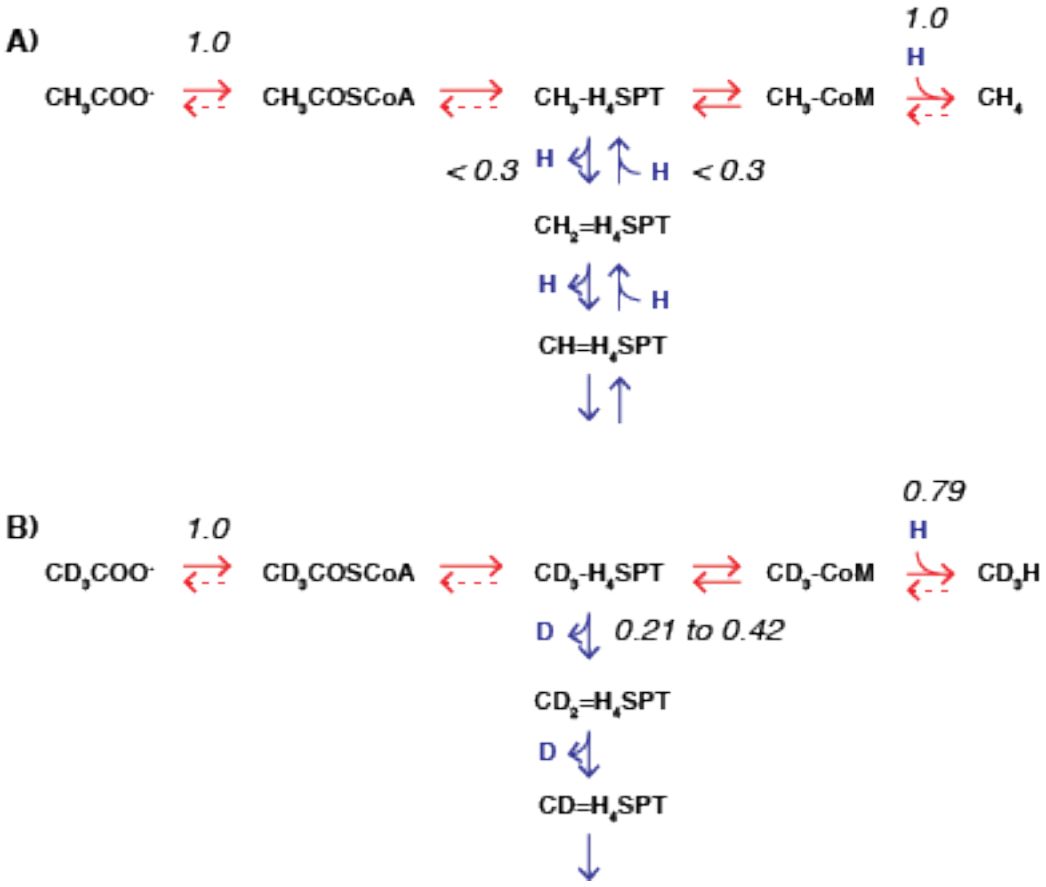

Figure 8: Proposed mechanism of D-isotope exchange by acetate metabolism by *M. barkeri*. The numbers in italics are relative fluxes estimated from A) D-spiked medium, and B) CD_3COO^- experiments, respectively. Reactions with two solid lines indicate that the reaction is thought to be reversible, whereas reactions with solid and dashed lines indicate that the reaction proceeds predominantly the direction of the solid arrow. As in Figure 7, the solid arrows represent the predominant direction of the reaction, and the dashed arrows represent the backward reaction. Red lines indicate the reactions required for the acetoclastic pathway. Blue lines indicate side reactions.

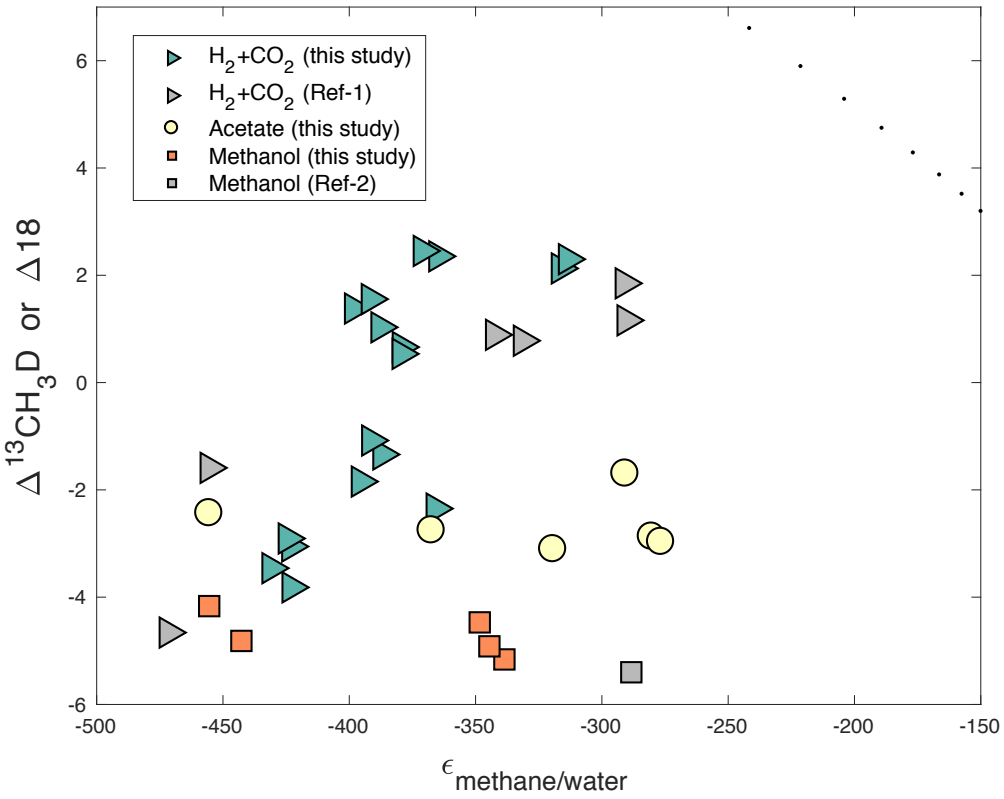

Figure 9. The values of D13CH3D (or D18) of methane plotted against D/H fractionation factor between methane and water ($\varepsilon_{methane/water}$) for methanogen cultures grown on different substrate. All culture data previously published with corresponding δD_{H2O} values is included for reference (grey symbols). Ref-1 refers to Stolper et al. (2015) and Ref-2 refers to Douglas et al. (2016). Black dots represent isotopic equilibrium (Wang et al., 2015).

Table 1. Summary of experiments.

Experiment (Method)	Organism(s)	Purpose	Variables	Substrates Used	Presented in
Temperature Series* (2.1.1)	*Methanocaldococcus jannaschii, Methanocaldococcus bathoardescens, Methanothermococcus thermolithotrophicus*	Effect of growth temperature	Growth Temperature	H_2+CO_2	Figures 1, 9 Tables 2, 3
Time Series (2.1.2)	*Methanocaldococcus bathoardescens*	Closed system isotope effects	Incubation Time	H_2+CO_2,	Figures 1, 2, 9 Tables 2, 3
Substrate Series (2.1.3)	*Methanosarcina barkeri, Methanosarcina mazei*	Substrate & Pathway effects	Substrate	H_2+CO_2, acetate, methanol	Figures 1, 3, 4, 5, 9 Tables 2, 3
Deuterated Water (2.1.4)	*Methanosarcina barkeri*	Hydrogen source	δD Water	H_2+CO_2, acetate, methanol	Figures 1, 3, 5, 6, 8, 9 Tables 2, 3
Deuterated Acetate (2.1.5)	*Methanosarcina barkeri*	Hydrogen source	CD_3COOD Spike	acetate	Figures 1, 4, 8, 9 Tables 2, 3

*A part of this data was reported in Wang et al. (2015) as noted in Table 2.

Table 2. Results for methanogen culture experiments.

Methanogen	Substrate*[1]	T (°C)	δD_{H2O}	$\delta^{13}C_{CH4}$	+/- ‰	δD_{CH4}	+/- ‰	$\Delta^{13}CH3D$	+/- ‰	Incubation (hrs)	Methane (mL)*[7]
Temperature Series Experiments (TS)											
M. jannaschii[*4]	H_2+CO_2	80	-49.0	-18.79	0.03	-415.46	0.05	2.29	0.23	5.25[*5]	NA
M. bathoardescens[*4]	H_2+CO_2	85	-49.0	-12.58	0.07	-417.80	0.07	1.03	0.45	8[*5]	NA
M. thermolithotrophicus[*4]	H_2+CO_2	40	-49.0	-16.47	0.04	-427.76	0.04	1.38	0.34	28[*5]	NA
M. thermolithotrophicus	H_2+CO_2	30	-49.0	-17.05	0.08	-421.44	0.12	1.56	0.28	64[*5]	NA
M. thermolithotrophicus	H_2+CO_2	60	-49.0	-17.15	0.06	-409.77	0.05	0.66	0.28	6[*5]	NA
M. thermolithotrophicus[*4]	H_2+CO_2	60	-49.0	-17.05	0.05	-409.84	0.05	0.54	0.28	6[*5]	NA
Time Series Experiments (CS)											
M. bathoardescens	H_2+CO_2 (6%)	80	-49.6	-17.82	0.07	-350.30	0.21	2.13	0.29	2.75	NA
M. bathoardescens	H_2+CO_2 (10%)	80	-49.6	-18.25	0.10	-347.63	0.10	2.30	0.55	3.25	NA
M. bathoardescens	H_2+CO_2 (68%)	80	-49.6	-3.91	0.04	-396.41	0.04	2.35	0.21	3.5	NA
M. bathoardescens	H_2+CO_2 (77%)	80	-49.6	-3.74	0.03	-402.25	0.03	2.45	0.29	4	NA
***Methanosarcina* Substrate, Spike, and Temperature Experiments - set 1[3]**											
M. barkeri[*4]	H_2+CO_2	21-38	-51.2	-59.90	0.05	-418.40	0.05	-1.34	0.22	336[*6]	NA
M. barkeri[*4]	H_2+CO_2	21-38	-51.2	-59.30	0.07	-422.67	0.07	-1.08	0.63	336[*6]	NA
M. barkeri	H_2+CO_2	21-38	100[*3]	-59.15	0.06	-340.47	0.05	-1.32	0.23	336[*6]	NA
M. barkeri	H_2+CO_2	21-38	260[*3]	-60.93	0.11	-201.10	0.11	-2.35	0.56	336[*6]	NA
M. barkeri	methanol	21-38	-51.2	-116.30	0.11	-372.46	0.11	-5.16	0.48	336[*6]	NA
M. barkeri	acetate	21-38	-51.2	-66.83	0.08	-317.08	0.09	-2.87	0.42	336[*6]	NA
M. barkeri	acetate	21-38	-51.2	-66.78	0.34	-313.61	0.55	-2.97	1.49	336[*6]	NA
***Methanosarcina* Substrate, Spike, and Temperature Experiments - set 2**											
M. barkeri	H_2+CO_2	38	85.4	-62.02	0.05	-373.86	0.05	-3.06	0.28	730	22
M. barkeri	H_2+CO_2	38	322.1	-58.08	0.05	-239.13	0.05	-2.91	0.23	730	39
M. barkeri	H_2+CO_2	38	-50.5	-57.40	0.05	-452.14	0.05	-3.82	0.32	730	30
M. barkeri[*2]	H_2+CO_2	21	-49.4	-70.52	0.05	-425.43	0.05	-1.85	0.23	730	15
M. barkeri	methanol	38	-39.1	-117.01	0.05	-370.16	0.05	-4.92	0.40	72	22
M. barkeri	methanol	38	196.7	-116.32	0.06	-333.09	0.06	-4.82	0.27	72	33
M. barkeri	methanol	38	334.7	-118.10	0.05	-273.19	0.06	-4.17	0.36	72	96
M. barkeri	acetate	38	105.1	-73.74	0.07	-300.93	0.07	-2.75	0.47	730	11
M. barkeri	acetate	38	359.7	-67.68	0.05	-259.54	0.05	-2.43	0.22	730	9
M. barkeri	acetate (+YE)	38	-35	-72.86	0.10	-343.12	0.10	-3.10	0.45	730	12
M. mazei	H_2+CO_2	38	-51.1	-56.07	0.05	-460.03	0.05	-3.46	0.22	730	23
M. mazei	acetate	38	-34.1	-60.40	0.05	-314.90	0.05	-1.70	0.20	730	11
M. mazei	methanol	38	-23	-120.82	0.04	-363.34	0.04	-4.47	0.20	72	86

*[1] Substrate (%) refers to the percent of substrate consumed or reaction completion.
*[2] The culture was grown at 21°C and excluded from Figure 3, 4 and analysis.
*[3] δD_{H2O} values represent estimates. These were measured for Set 2.
*[4] From Wang et al., 2015
*[5] Values represent an estimate based on previous culture data using this this culture strain grown at similar temperatures.
*[6] Values represent estimated incubation time.
*[7] Volume of methane (STP) in the culture headspace at the end of the incubation time. NA is recorded for all cultures that were not injected with NaOH at the end of incubation and prior to isotope measurements.

Table 3. Isotopic compositions of substrates and medium water.

Material	$\delta^{13}C$ ‰	δD_{H2O} ‰	δD_{CH3} ‰
H_2 - CO_2 gas mix*[1]	-34.4		
N_2 - CO_2 gas mix*[1]	-35.8		
CH_3COONa[1]	-40.2		-123
CH_3OH*[1]	-49.5		
Bremen DI Water*[2]		-51.2	
UMass DI Water*[3]		-49.6	

*1: These materials were used for Set 2 of substrate and D-spike experiments.
*2: Bremen DI water (pre-inoculation) was used in Set 2 of substrate and D-spike experiments.
*3: UMass DI water (pre-inoculation) was used in the temperature and time-series experiments.